





37 1. Introduction

38 Mesopause is one of the complex and intricate domain regions of Earth's atmosphere. It is the  
39 thermal transition area that plays an important role in the vertical coupling of the Earth's  
40 atmosphere. In the global mean temperature, mesopause is the coldest layer of the  
41 atmosphere (Zhao et al., 2020; Ortland et al., 1998). Polar summer mesopause is considered  
42 the coldest place on Earth (Ortland et al., 1998). The region has several unique physical and  
43 chemical characteristics including the complex interplay between radiative transfer,  
44 dynamics, and photochemistry (Smith, 2004). The height of the mesopause is not constant but  
45 varies significantly with latitude and season (Xu et al., 2007; Wang et al., 2022). The height  
46 is approximately 90 and 100 km in summer and winter respectively (Brasseur and Solomon,  
47 2005). At mid and high latitudes the mesopause is located near 85km during the summer  
48 season (Smith, 2004). The mesopause of the high- and middle-latitude regions is at a lower  
49 and higher altitude in summer (around the summer solstice) and in winter/other seasons  
50 respectively. The mesopause is at a higher altitude at the equator for all seasons (Xu et al.,  
51 2007).

52 Spatial and temporal variability in temperature exists in the vertical temperature profile as  
53 well as changes with changing latitude. The temperature at the mesopause region exhibits a  
54 robust temporal variation (Mulligan et al., 1995; Offermann et al., 2010; Clancy and Rusch,  
55 1989; Hedin, 1991; Dyrland et al., 2010; She et al., 2000; French et al., 2020b; Dalin et al.,  
56 2020; Grygalashvyly et al., 2014). Long-term and short-term temperature trends were studied  
57 by (Beig, 2011a, 2011b; Kalicinsky et al., 2016; Pancheva et al., 2013; She et al., 2015;  
58 Venkat Ratnam et al., 2010; Wörl et al., 2019; Xu et al., 2007; and recently reviewed by Gul  
59 2024). Short-term variability in temperature is primarily due to small-scale gravity waves and  
60 tides (Dalin et al., 2017; Zhao et al., 2020). Air temperature measurements from the  
61 mesopause layer have long been important (Jarvis, 2001), because the cold temperatures of  
62 this layer are the potential tracers of the dynamics (Beig et al., 2003). The temperature during  
63 summer at the pole ranges between 120 to 140 K and at the winter pole range between 180 to  
64 210 K (Brasseur and Solomon, 2005; Gul, 2024). This indicates that summer polar  
65 mesopause receives significantly more solar radiation as compared to winter mesopause, but  
66 the temperature is lowest at summer polar mesopause observed anywhere on Earth. The  
67 temperature response to solar activity is  $\sim +2$  times greater in winter than in summer (Dalin et  
68 al., 2020). Winter mesopause temperature trends ( $-6$  to  $-2$  K/decade) are generally stronger  
69 than summer ones ( $-2$  to  $+0.5$  K/decade (Offermann et al., 2010). Gravity and planetary



70 waves (Dalin et al., 2017), and atmospheric tides (Smith, 2004) bring periodic variations in  
71 temperature.

72 WV is one of the strongest greenhouse gases in the atmosphere, important for cloud  
73 formation, and plays a crucial radiative balance role in the atmosphere. WV in the upper  
74 atmosphere can affect global surface climate (Solomon et al., 2010). WV in the atmosphere  
75 regulates the Earth's weather and climate (Wallace and Hobbs, 2006). WV's existence in the  
76 polar summer mesopause is of critical importance because it combines with the lowest  
77 temperature of the mesopause region to enable noctilucent clouds (NLCs) to form. The  
78 increased occurrence of NLC and its appearance is an indication of global change (Russell III  
79 et al., 2014). Knowledge of WV distribution in the upper atmosphere is highly valuable for  
80 understanding the respective roles of atmospheric chemistry, atmospheric dynamics, and  
81 climate change. Complete methane (CH<sub>4</sub>) oxidation is one of the major sources of WV  
82 (Brasseur and Solomon, 1986). In the mesopause region, more abundant WV from increasing  
83 CH<sub>4</sub> contributes to more frequent NLC occurrences (Lübken et al., 2018). The rocket  
84 measurements gave water-mixing ratios of 3 to 7 ppm ranging between 40 and 70 km altitude  
85 (Rogers et al., 1977). The airborne observation gave a water mixing ratio of 4 to 5 ppm at the  
86 altitude range between 40 and 80 km (Waters et al., 1977). WV content in the atmosphere  
87 controls the concentration of O<sub>3</sub> that, in turn, affects mesospheric cooling. The Photochemical  
88 lifetime of H<sub>2</sub>O is relatively long making it an excellent tracer for atmospheric dynamics  
89 (Peter, 1998) enabling one to follow the atmospheric transport effects up to high altitude  
90 regions (80–85 km). The seasonal and long-term changes in mesospheric WV are discussed  
91 by (Chandra et al., 1997). Due to the high sensitivity of WV to temperatures, NLC  
92 phenomena can be used as temperature probes in the mesopause region (Lübken et al., 2007;  
93 Petelina and Zsetsky, 2009) and as possible indicators of climate change (Thomas, 2003).  
94 As compared to temperature, there have been fewer observations of WV in the upper  
95 mesosphere.

## 96 2. Methodology

### 97 2.1 Study area

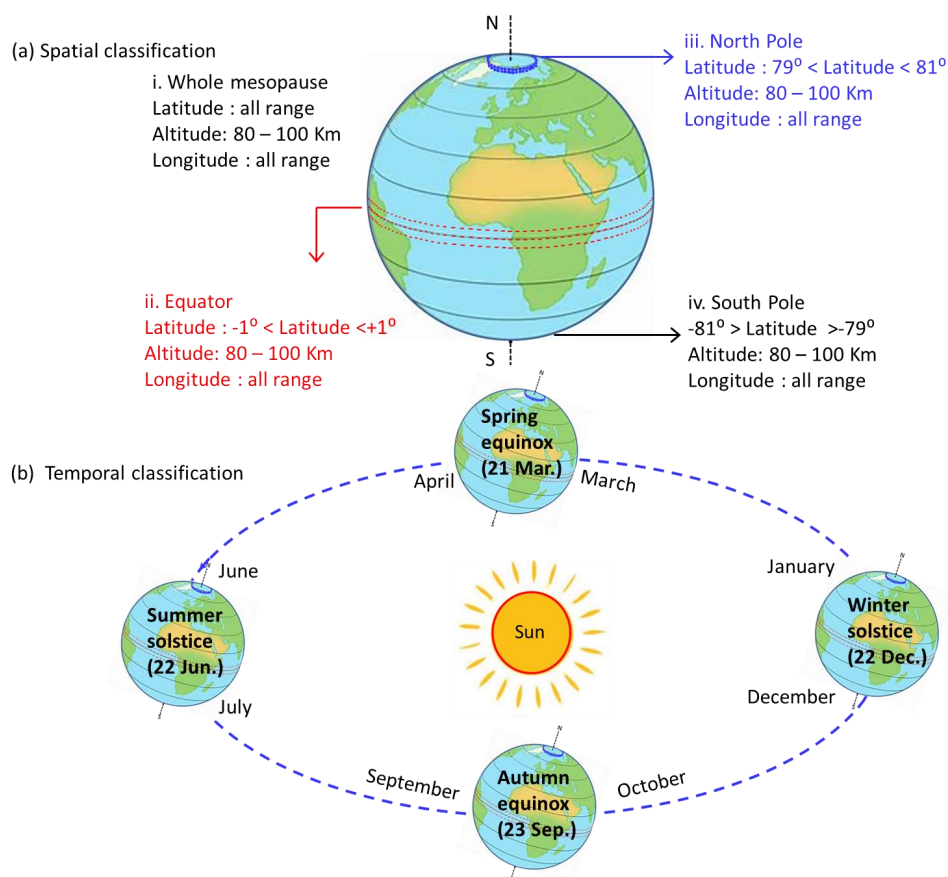
98 Temporal and spatial variations of temperature and WV were monitored in the mesopause  
99 region (Figure 1). Spatially the region was divided into four parts (North Pole, Equator, and  
100 South Pole). Two two-degree latitude areas were selected for all longitude ranges (Figure 1).  
101 Temporally twenty-two years (2002 - 2023) selected monthly data (as shown in Figure 1b)  
102 was used from the TIMED SABER instrument. We used kinetic temperature (K) and H<sub>2</sub>O



103 Mixing Ratio (ppmv) having dimensions of altitude, the event from SABER Custom Level2A  
104 Product (Processed Level2A). We have excluded the four transitional months (November,  
105 February, May, and August) and included four equinox months (March, April, September,  
106 and October), and four solstice months (January, December, June, and July). We select  
107 summer /northern hemisphere (NH) at  $\sim 80^\circ \pm 1^\circ$  latitude, equator at  $\sim 0^\circ \pm 1^\circ$  latitude, and  $80^\circ$   
108  $\pm 1^\circ$  latitude in the winter/southern hemisphere (SH) for interannual variations of temperature  
109 and WV during the study period. Temperature and WV trends are presented and compared  
110 among different latitudinal and seasonal ranges. There is missing data in almost every  
111 latitude (Zhu et al., 2005), particularly at high latitudes that vary with season. We applied a  
112 weighted average to fill  $\sim 40\%$  of missing values.

### 113 2.2 TIMED SABER instrument

114 SABER provides an excellent quality of the measured infrared limb radiances (Esplin et al.,  
115 2023). SABER is an infrared limb-sounding instrument used for atmospheric sounding and  
116 observing the atmosphere around the mesopause region continuously for over two decades.  
117 Technical description of the SABER instrument and further relevant information are  
118 discussed by Esplin et al., (2023); Mlynczak, (1997); and Russell III et al., (1999). Due to a  
119  $\sim 60$ -day yaw cycle of the TIMED satellite, the latitude coverage shifts between  $83^\circ\text{N}$ – $53^\circ\text{S}$   
120 and  $53^\circ\text{N}$ – $83^\circ\text{S}$ . TIMED satellite rotates  $180^\circ$  about its yaw axis and provides latitude  
121 coverage continuously in the range of  $53^\circ\text{S}$  to  $83^\circ\text{N}$  and then switching to  $83^\circ\text{S}$  to  $53^\circ\text{N}$  every  
122  $\sim 60$  days (Russell III et al., 1999). NASA-TIMED SABER instrument is performing near-  
123 global measurements of the vertical kinetic temperature profiles along with volume mixing  
124 ratios of WV. The random error of the v2.07 for SABER H<sub>2</sub>O product is 30% at 80km  
125 altitude and further increases with increasing attitude (Rong et al., 2019). The rapid increase  
126 in error is mainly due to low signal-to-noise. The estimated systematic error of SABER  
127 version 2.07 H<sub>2</sub>O is about 10- 20%.



128

129 Figure 1. Study area (a) spatial range of selected regions, (b) temporal range from selected  
130 years from 2002 to 2023.

### 131 3. Results

#### 132 3.1. Variation in temperature and water vapor in the whole mesopause region

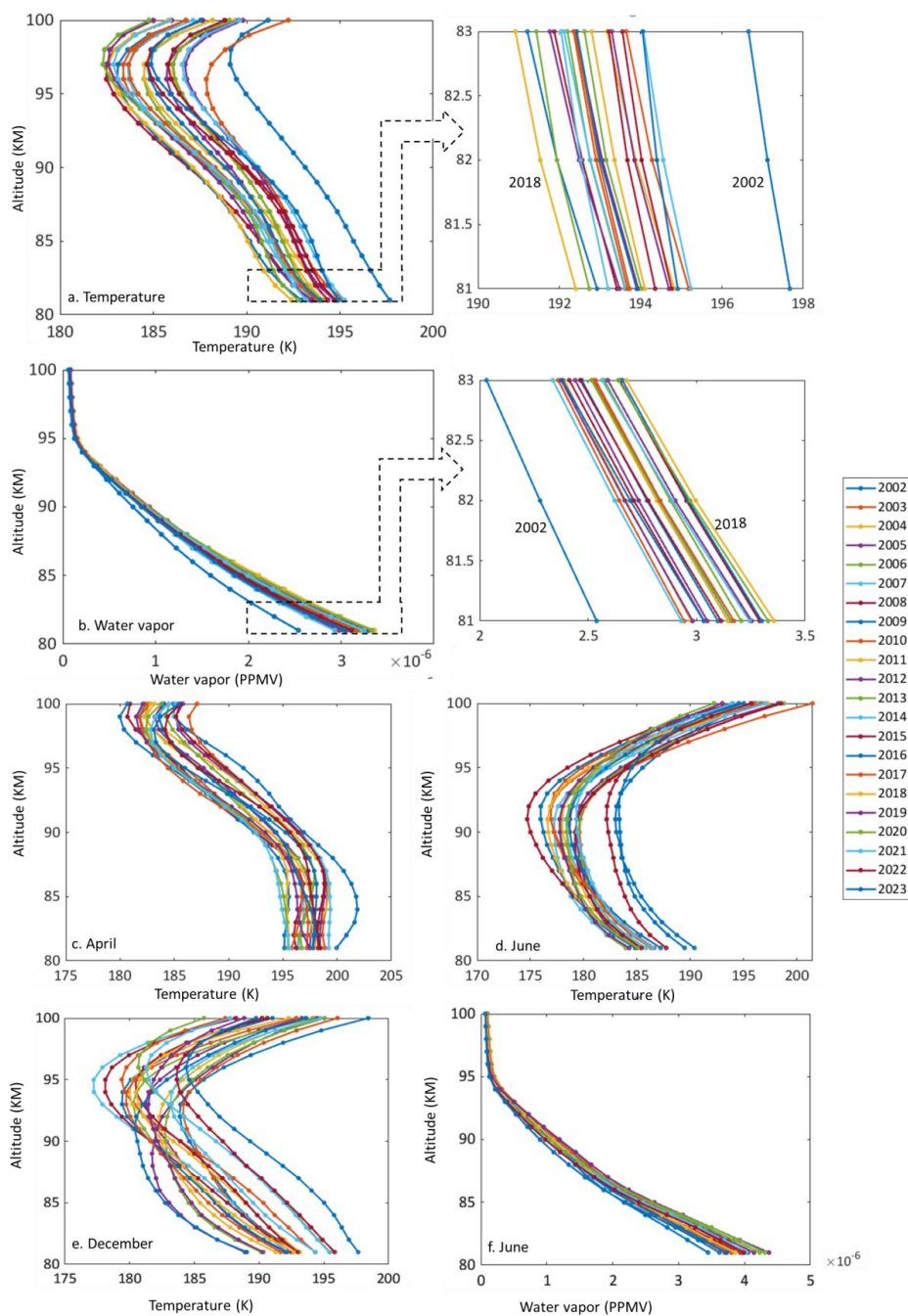
133 It is well known that temperature and WV in the atmosphere have high variability in space  
134 and time. The vertical profiles of yearly averaged (selected 8 months averaged) temperature  
135 and WV gradient with respect to mesopause altitude (km) are plotted in (Figure 2), described  
136 in the following sections.

##### 137 3.1.1 Variation in temperature

138 The year 2002 was the hottest (~193K) followed by 2003 (191K) and 2018 was the coldest  
139 (~187K) year followed by 2008 (187.1K) during the study period Figure 2a. Yearly averaged  
140 temperature decreased by ~6K from 2002 to 2008 and increased by ~3K from 2009 to 2012.



141 A second decrease in temperature  $\sim 4\text{K}$  was observed from 2014 to 2018. A decreasing trend  
142 in temperature was observed  $\sim 0.37\text{K}$  decrease from 2002 to 2018 and  $\sim 0.14\text{K}$  decrease  
143 during the whole study period 2002-2023. A decreasing trend in temperature (different  
144 magnitude) was also reported by other authors in the past (Zhao et al., 2020; Dalin et al.,  
145 2020; Yuan et al., 2019; Hervig and Siskind, 2006; French et al., 2020a; Venkat Ratnam et  
146 al., 2010; Semenov et al., 2002). June 2008 ( $\sim 180\text{K}$ ) followed by July 2009 ( $\sim 181\text{K}$ ) were the  
147 coldest months and January 2002 ( $\sim 197\text{K}$ ) was the hottest month during the study period.  
148 March (max:  $196.8\text{K}$  min:  $188.3\text{K}$  avg:  $191.4\text{K}$ ), April (max:  $195.2\text{K}$  min:  $189.6\text{K}$  avg:  $192\text{K}$ ),  
149 September (max:  $195.7\text{K}$  min:  $187.8\text{K}$  avg:  $190.6\text{K}$ ), and October (max:  $195.8\text{K}$  min:  $189.3\text{K}$   
150 avg:  $191.7\text{K}$ ) were relatively hotter months as compared to June and July. The monthly  
151 averaged temperature at two equinoxes (Mar/Apr and Sep/Oct) were  $191.66\text{K}$  and  $191.16\text{K}$   
152 respectively. Similar monthly temperature patterns (lower temperatures during June and July)  
153 were also reported in the past such as (Dalin et al., 2020; French et al., 2020; Offermann et  
154 al., 2010). Therefore, seasonal temperature variations at the mesopause region are distinct,  
155 with a summer minimum (June  $\sim 180\text{K}$ , July  $\sim 183\text{K}$ ) and a winter maximum (January  
156  $\sim 197\text{K}$ , December  $\sim 190\text{K}$ ). The monthly averaged temperatures at two solstices (Jun/July and  
157 Dec/Jan) were  $184.55\text{K}$  and  $188.20\text{K}$  respectively, indicating the coldest temperature during  
158 June and July throughout the whole study period. Mesopause during the summer (June and  
159 July) solstice is  $\sim 3.65\text{K}$  colder than that during the winter (December and January) solstice  
160 ( $\sim 6\text{--}9\text{K}$  colder was reported by Wang et al., (2022) and Xu et al., (2007). The seasonal  
161 temperature variation is characterized by temporal variability in harmonics (Ammosov et al.,  
162 2014; Kalicinsky et al., 2016; Perminov et al., 2014). Air is drawn downward in winter and  
163 upward in summer keeping away mesopause from thermodynamic equilibrium. As a result,  
164 the mesopause is kept away from thermodynamic equilibrium, with very low temperatures in  
165 summer (June and July) and relatively high temperatures in winter (January and December).  
166 The difference in temperature and the greater solar flux in December/January than in  
167 June/July may also be due to the Earth's orbital eccentricity, as discussed by Chu et al.,  
168 (2003).



169

170 Figure 2. Variation of temperature and water vapor in the mesopause region during 2002-  
171 2023 for the whole mesopause region.



172 Rising air expands and cools, resulting in a chilly summer mesopause, while downwelling air  
173 compresses and warms, resulting in a warm winter mesopause. Downwelling in the winter  
174 hemisphere and upwelling in the summer hemisphere causes adiabatic warming, and the  
175 causes adiabatic cooling (States and Gardner, 2000; Xu et al., 2007). The transport of CO<sub>2</sub>  
176 affects the infrared cooling rate in the upper atmosphere leading to globally warmer  
177 mesopause temperatures (Chabrilat et al., 2002) and enhanced differences in temperature  
178 between the winter and summer. An analysis based on the work of (Dopplick, 1972; Kuhn  
179 and London, 1969; López-Puertas et al., 1992), shows that the maximum cooling rate by CO<sub>2</sub>  
180 is found during the winter mesopause, where the temperature is relatively high. Thermal  
181 infrared cooling is associated with WV, CO<sub>2</sub>, and ozone and is a vital function of temperature  
182 (Brasseur and Solomon, 2005). Mesospheric residual circulation is responsible for relatively  
183 cold summers and warm winters. Temporal temperature variations may also be caused by  
184 several factors including changes in the SOI-index, changes in the indices of geomagnetic  
185 and solar activity (Medvedeva and Ratovsky, 2023), planetary, atmospheric, and meridional  
186 circulation driven by breaking gravity waves (Offermann et al., 2009, 2011; Perminov et al.,  
187 2014; Smith, 2012).

188 Temperature is also changing with respect to the change in altitude of the mesopause region.  
189 Overall averaged temperature at 80km altitude was maximum (194.11K) and decreased by  
190 ~10K up to (184.72K) at the altitude of 97km as shown in Figure 2a. In general, lower  
191 mesopause regions (80 – 90km) are relatively hotter than the upper part of mesopause (90-  
192 100km). This temperature gradient was not consistent/similar for all selected months.  
193 Different months showed slightly different patterns of temperature change with respect to  
194 changing altitudes shown in Figure 2. Patterns of solstices (summer, and winter) were  
195 different from the two equinoxes (Figure 2c, d, e). The temperature variation in June and  
196 April (Figure 2c, d) are similar to the temperature variation in December (Figure 2e)  
197 respectively.

198

### 199 3.1.2 Variation in water vapor

200 In the mesopause region, large fractional temporal and spatial variations in WV were  
201 observed. Based on the monthly averaged WV for selected eight months of data, 2018 had a  
202 relatively higher amount of water content (~1.14ppmv) followed by 2008 (1.14ppmv), and  
203 2002 has the least amount of WV (~0.89ppmv) year followed by 2014 and 2003 (~1.0 ppmv)  
204 during the study period Figure 2b. Overall an increasing trend in WV was observed





205 ~0.13ppmv during the whole study period 2002-2023 (Figure 3a). An increasing trend in WV  
206 was also reported by other authors in the past (Huaman and Balsley, 1999). WV content in the  
207 mesopause region was in the range of ~ 0.05 ppmv(December 2009 at 100km altitude)–  
208 4.81ppmv (June 2019 at 80km altitude) relatively smaller variation than previously reported  
209 values ~0.1-10ppmv by other authors in the past (Berger and Von Zahn, 2002; Von Zahn and  
210 Berger, 2003; Lubken et al., 2004; Lübken et al., 2009; Körner and Sonnemann, 2001;  
211 Sonnemann et al., 2005). July 2008 (~1.48ppmv) followed by June 2019 (~1.45ppmv) were  
212 the months had maximum WV content and April 2002 (~0.61ppmv) followed by October  
213 2002 (~0.61ppmv) had minimum WV content during the study period. Monthly averaged  
214 WV at two equinoxes (March/April and September/October) were 0.85ppmv and 0.88ppmv  
215 respectively. In the mesosphere, the SABER H<sub>2</sub>O increasing trend was 0.1–0.2 ppmv per  
216 decade (Yue et al., 2019), however, we observed a relatively lower increasing trend at the  
217 equator (~0.09) and South Pole (~0.08) and North Pole (~0.06) ppmv/decade. An increasing  
218 trend in WV in the lower atmosphere was also reported by (Oltmans and Hofmann, 1995;  
219 Oltmans et al., 2000; Hurst et al., 2011; Nedoluha et al., 2013; Remsberg et al., 2018). The  
220 Mesopause region showed a distinct pattern, with a summer maximum (June ~ 1.45ppmv,  
221 July ~1.48ppmv) and a winter minimum (April ~0.61, October ~0.61ppmv). Monthly  
222 averaged WV at two solstices (Jun/July and December/January) were 1.32ppmv and  
223 1.23ppmv respectively. Nedoluha et al., (2022) showed maximum WV content during June  
224 and July at 80km altitude. WV in the polar region is relatively higher in summer than in  
225 winter. This may be due to upwelling in the summer hemisphere transports WV from lower  
226 altitudes towards the mesopause (Körner and Sonnemann, 2001). There is no clear insitu  
227 source of WV in the mesopause, except transported upwards from the stratosphere via the  
228 meridional circulation and eddy transport, because of prevailing meridional circulation, and  
229 Methane oxidation.

230 WV content is also changing with respect to the change in altitude of the mesopause region.  
231 Overall averaged WV content at ~80km altitude was maximum (~3.16ppmv) and decreased  
232 by ~3ppmv up to (~0.1ppmv) at the altitude of 97km as shown in Figure 2b. At 80 km  
233 altitude, the WV mixing ratio ranges from ~ 1.5 to 4.5 ppmv reported by (Seele and Hartogh,  
234 1999). In general, lower mesopause regions (80 – 83km) have relatively more WV content  
235 than upper part of mesopause (84-100km). On average altitude above, 95km has very little  
236 content of WV ~0.75ppmv. There are few studies including (Hervig et al., 2003) which  
237 showed WV enhancement above 86 km altitudes. There is a distinct annual cycle of the WV



238 mixing ratio that can be seen in the three selected latitude ranges. The seasonal increase in  
 239 WV is relatively more prompt at lower altitudes of the mesopause region. The variations  
 240 (spatial and temporal) in atmospheric WV can be largely explained by dynamical factors  
 241 (quasi-biennial oscillation, the Brewer-Dobson circulation, and temperature changes)  
 242 (Dessler et al., 2014). The amount of WV in the region can also change with solar-cycle-  
 243 induced variations in Lyman- $\alpha$  radiation (Hervig and Siskind, 2006; Nedoluha et al., 2009).  
 244 On the solar cycle time scale, H<sub>2</sub>O may vary by about 30-40% near the mesopause height  
 245 (~80 km) caused by the solar cycle modulation of Lyman alpha (Chandra et al., 1997). At  
 246 mesospheric heights, WV is strongly photo-dissociated by solar Lyman alpha (Brasseur and  
 247 Solomon, 1986). Solar cycle UV changes will have a strong influence on the long-term  
 248 changes in WV. Therefore, The solar cycle does play an important role in upper mesospheric  
 249 WV (Nedoluha et al., 2022). Additionally, changes in surface CH<sub>4</sub> emissions can increase the  
 250 amount of WV in the region due to CH<sub>4</sub> oxidation (Le Texier et al., 1988; Wrotny et al.,  
 251 2010). The secular increase in H<sub>2</sub>O related to methane increase in the atmosphere is about  
 252 0.4% /year at all heights in the mesosphere (Chandra et al., 1997). Model results suggest that  
 253 the temporal changes in mesosphere WV are largely controlled by the vertical advection  
 254 process associated with the meridional circulation (Chandra et al., 1997). The photolysis  
 255 process destroys H<sub>2</sub>O towards higher altitudes. The mesospheric WV content is the result of  
 256 the balance between its photodissociation and the upward transport from the stratosphere.  
 257 Temperature and WV content comparisons with past studies are shown in Table 1.

258

259 Table 1. Temperature and water vapor content comparisons with past studies in mesopause

	Altitude(km)	Method / Location/Instrument	Reference
Temperature/trend			
195K	80	TIMED SABER instrument	This study
189K	90	TIMED SABER instrument	This study
188K	100	TIMED SABER instrument	This study
-4K/decade	80-100	North Pole - TIMED SABER instrument	This study
-1.5K/decade	80-100	South Pole - TIMED SABER instrument	This study
-3K/decade	mesopause	LIMA model simulation	(Berger and Lübken, 2011)
-0.23K/year	87	GRIPS I and GRIPS II (small grating spectrometers of moderate resolution)/ Wuppertal (51°N, 7°E)	(Offermann et al., 2010), summer
-0.89K/year	mesopause region	Ground-based Infrared P-branch Spectrometer (GRIPS)/ Wuppertal (51°N, 7°E)	(Kalicinsky et al., 2016)
-2.5K/decade	92-97	The Na lidar at Fort Collins, CO (41°N, 105°W), and at Logan, UT (42°N, 112°W)	(Yuan et al., 2019)
-2.4K/decade	mesopause	OH* rotational temperature	(Dalin et al., 2020), summer
-0.4K/decade	mesopause	Moscow (Russia) ~57°N, 37°E	(Dalin et al., 2020), winter
-1.2K/decade	mesopause	LIMA and MIMAS model simulations 55–61°N	(Lübken et al., 2018)
-6.8K/decade	100	TIMED SABER instrument	(She et al., 2009)
-1.5K/decade	91	TIMED SABER instrument	(She et al., 2009)



-2.9K/decade	80–105 km	Na lidar (41°N, 105°W)	(She and Krueger, 2004)
-2.1K/decade	mesopause	OH(6-2) rotational temperature (63°N)	(Ammosov et al., 2014)
-2K/decade	mesopause	OH* model simulations,	(Grygalashvyly et al., 2014)
-0.22K/year	mesopause	Airglow measurement	(Perminov et al., 2014)
-0.24K/decade	80 - 88 km	Model simulations	(Hervig et al., 2015)
-0.5K/decade	mesopause	Model simulations	(Hervig et al., 2016)
-2K/decade	mesopause	Whole Atmosphere Community Climate Model eXtended (WACCM-X)	(Yuan et al., 2019)
-1.2K/decade	mesopause	OH nightglow rotational temperature	(French et al., 2020)
-0.3K/decade	mesopause	TIMED/SABER and airglow	(Noll et al., 2017)
<b>Mixing ratio (ppmv)</b>			
3.65	80	TIMED SABER instrument	This study
0.88	90	TIMED SABER instrument	This study
0.07	100	TIMED SABER instrument	This study
0.06ppmv/decade	80-100	North Pole - TIMED SABER instrument	This study
0.08ppmv/decade	80-100	South Pole - TIMED SABER instrument	This study
~1.5	90	SOFIE on AIM satellite and ALOMAR lidar	(Hervig et al., 2009)a
1	90	Using classical nucleation theory and a one-dimensional model	(Murray and Jensen, 2010)
3	86	ion-chemical model (A model that aims to describe these processes must combine basic ion chemistry, clustering processes as well as charge capture by particles)	(Gumbel et al., 2003)
1	85	Ground-based microwave techniques	(Bevilacqua et al., 1983)
2.4	85	Ground-based microwave technique at Norway (69°N)	(Seele and Hartogh, 1999)
3.4	84	rocket-borne mass spectrometer (69°N, 16°E)	(Arnold & Krankowsky, 1977)
4	84	space-borne methods/ SBUV (solar backscatter ultraviolet) satellite instrument, 77°N	(Hervig et al., 2016)
3	83	3-D model / upper mesosphere at high latitudes, 60°N	(Von Zahn and Berger, 2003)
4	83	3D-Model/mesopause / Smolarkiewicz scheme	(Körner & Sonnemann, 2001)
1	83	HALOE measurement / polar summer mesosphere	(Hervig et al., 2003)
1	82	2-D numerical model	(Jensen and Thomas, 1994)
1.8	80	HALOE measurement /34°N	(Russell III et al., 1993)
<4	~80	HALOE measurement and chemical-dynamical model,	(Summers et al., 1997)
0.45 to 4.81	80-94	Model /Spitsbergen 78°N,	(Lubken et al., 2004)
3 to 5.6	79-89	Aura/MLS satellite /middle latitudes (45–50°N)	(Dalin et al., 2023)

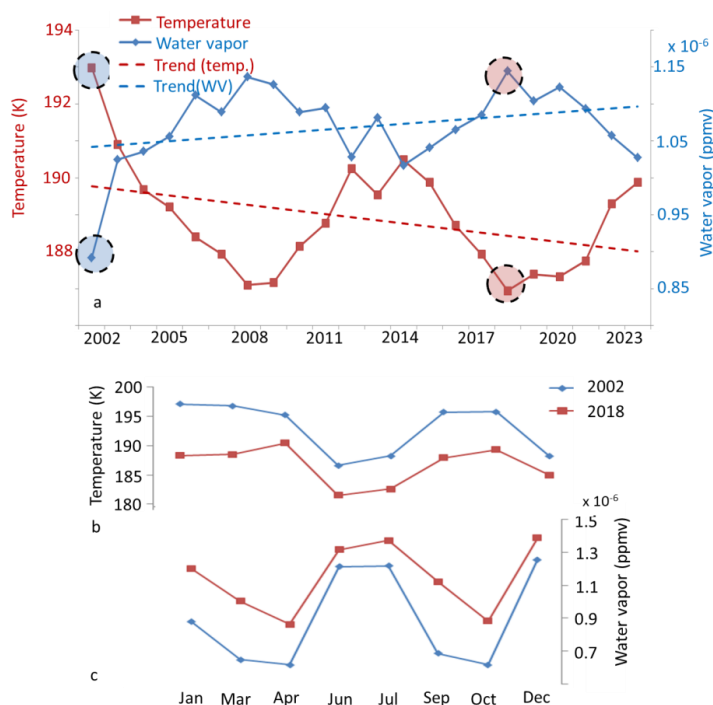
260

### 261 3.1.3 Relationship between temperature and water vapor

262 Temperature showed a decreasing trend (discussed in section 3.1.1) and WV showed an  
 263 increasing trend (discussed in section 3.1.2) indicating a strong negative correlation between  
 264 WV and temperature Figure 3. A similar negative relation between WV with the solar cycle  
 265 at an altitude of 82km was also shown by Yue et al., (2019) and (Dalin et al., 2023). WV  
 266 measurements showed a decadal cycle (2002-2011, and 2011-2023) that is anticorrelated with  
 267 temperature variability, showing relatively more H<sub>2</sub>O during solar minimum Figure 3. A  
 268 similar anticorrelated relation between WV and solar variability was observed by (Hervig  
 269 and Siskind, 2006), and showed ~25% more H<sub>2</sub>O during solar minimum. Figure 3a shows the



270 yearly averaged temperature and WV content, where the opposition relationship is visible.  
 271 The year 2002 (maximum averaged temperature) and 2018 (minimum averaged temperature)  
 272 were the two extrema temperature years and were further explored on the monthly level in  
 273 part b (Temperature) and part c (WV) of Figure 3. The opposite correlation between  
 274 temperature and WV is true for a specific altitude. With increasing altitude (80 to 100km)  
 275 temperature and WV content both decreased (Figure 2). The precise relationship between  
 276 WV saturation mixing ratios and cold point temperature depends upon the temperature as  
 277 well as exact pressure (altitude), with Seidel et al., (2001) giving a value of  $\sim 0.6$  ppmv/K,  
 278 (Fueglistaler and Haynes, 2005)  $\sim 0.5$  ppmv/K, and (Nedoluha et al., 1998)  $\sim 0.7$  ppmv/K. In  
 279 the present study, the maximum and minimum WV change between 81 to 100 km altitude  
 280 was  $\sim 4.3$  and  $\sim 1.6$  ppmv respectively. Solar cycle (temperature) variations impact on WV  
 281 and their relationship has been quantified by multiple researchers in the past (Brasseur and  
 282 Solomon, 1986; Chandra et al., 1997; Fiedler et al., 2011; Hervig and Siskind, 2006; Siskind  
 283 et al., 2013).



284

285 Figure 3. Relationship between temperature and water vapor content a. yearly averaged  
 286 temperature and water vapor in selected, b. temperature, c. water vapor for two selected  
 287 years.



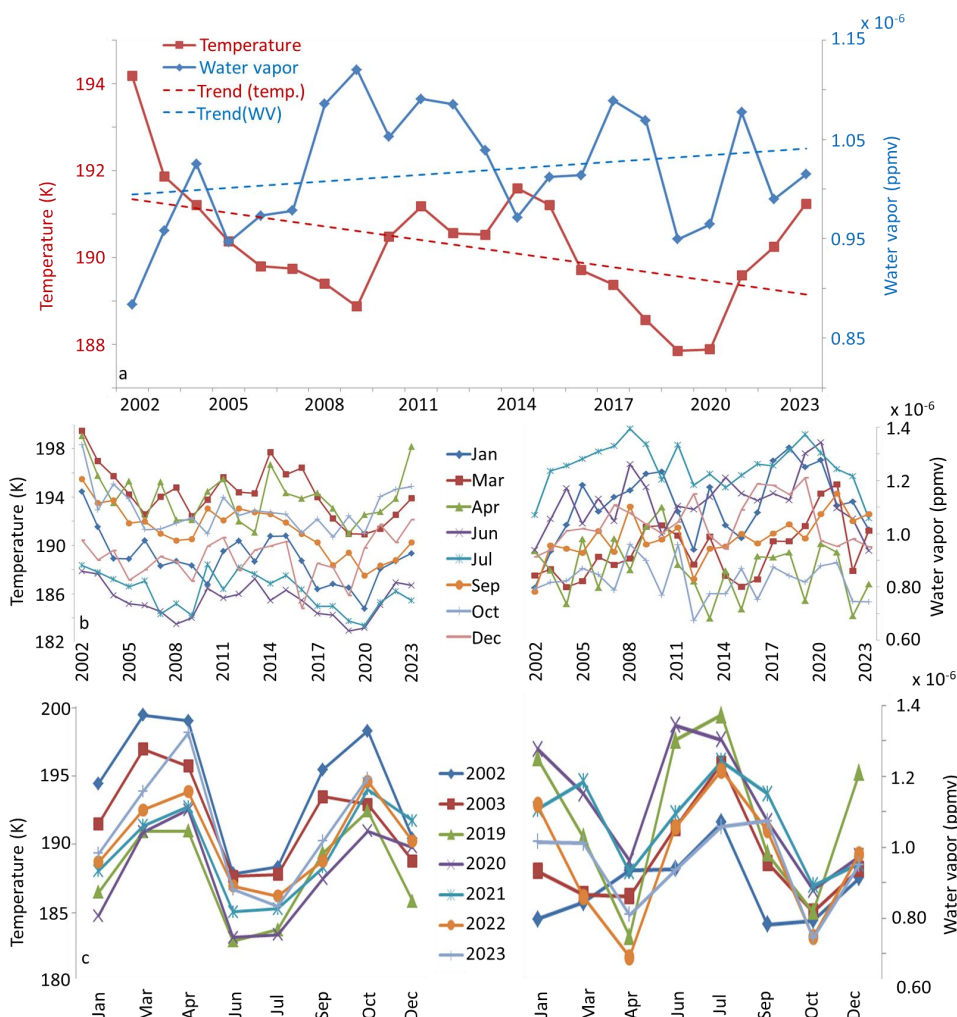
288

### 289 3.2 Temperature and water vapor variation over the equator

290 Monthly averaged temperature data for selected eight months data, 2002 (~194K) was the hottest,  
291 and 2019 (~188K) was the coldest year during the study period. June 2019 (~183K) was the coldest  
292 and March 2014 (~198K) was the hottest month. Overall, there is a decreasing trend of temperature  
293 (~1.5K/decade) over the equator. This decreasing trend in temperature is visible in all selected  
294 months, particularly during September where this change is more prompt as compared to June and  
295 July. The monthly averaged temperature at two equinoxes (Mar/Apr and Sep/Oct) were 194.15K and  
296 192.07K respectively. Similarly, monthly averaged temperatures at two solstices (Jun/July and  
297 Dec/Jan) were 185.81K and 188.95K respectively, indicating the coldest temperature during June and  
298 July and the hottest temperature during March and April throughout the study period. Temperature  
299 showed a decreasing trend with altitude in all selected months. Temperature decreased from 80 to 100  
300 km during June and July was up to 10K, and during other months was around 20K.

301 Similarly, based on the monthly averaged WV data for selected eight months data, 2002 (~0.88ppmv)  
302 followed by 2005 (~0.94ppmv) were the two least content WV years, and 2009 (~1.12ppmv) followed  
303 by 2011 (~1.09ppmv) were the two maximum content of WV years during the study period. On  
304 average July (1.25ppmv) had the maximum WV content followed by June (1.12ppmv) and October  
305 (0.82ppmv) followed by April (0.87ppmv) had the minimum WV content. Overall, there is an  
306 increasing trend of WV (~0.09ppmv/decade) over the equator of the mesopause region. The monthly  
307 averaged WV at two equinoxes (Mar/Apr and Sep/Oct) was almost the same 0.90ppmv.

308 Similarly, monthly averaged WV at two solstices (Jun/July and Dec/Jan) were 1.19ppmv and  
309 1.08ppmv respectively, indicating relatively high WV content during June and July. WV content at  
310 lower altitudes 81, 82, and 83km were 2.97, 2.65, and 2.36ppmv respectively, and decreased with  
311 altitude in all selected months. A decreasing trend in temperature and an increasing trend in WV is  
312 clear in Figure 4a (yearly averaged). Monthly averaged variations in temperature and WV are shown  
313 in Figure 4b, having a clear inverse relation in selected months and years Figure 4c.



314

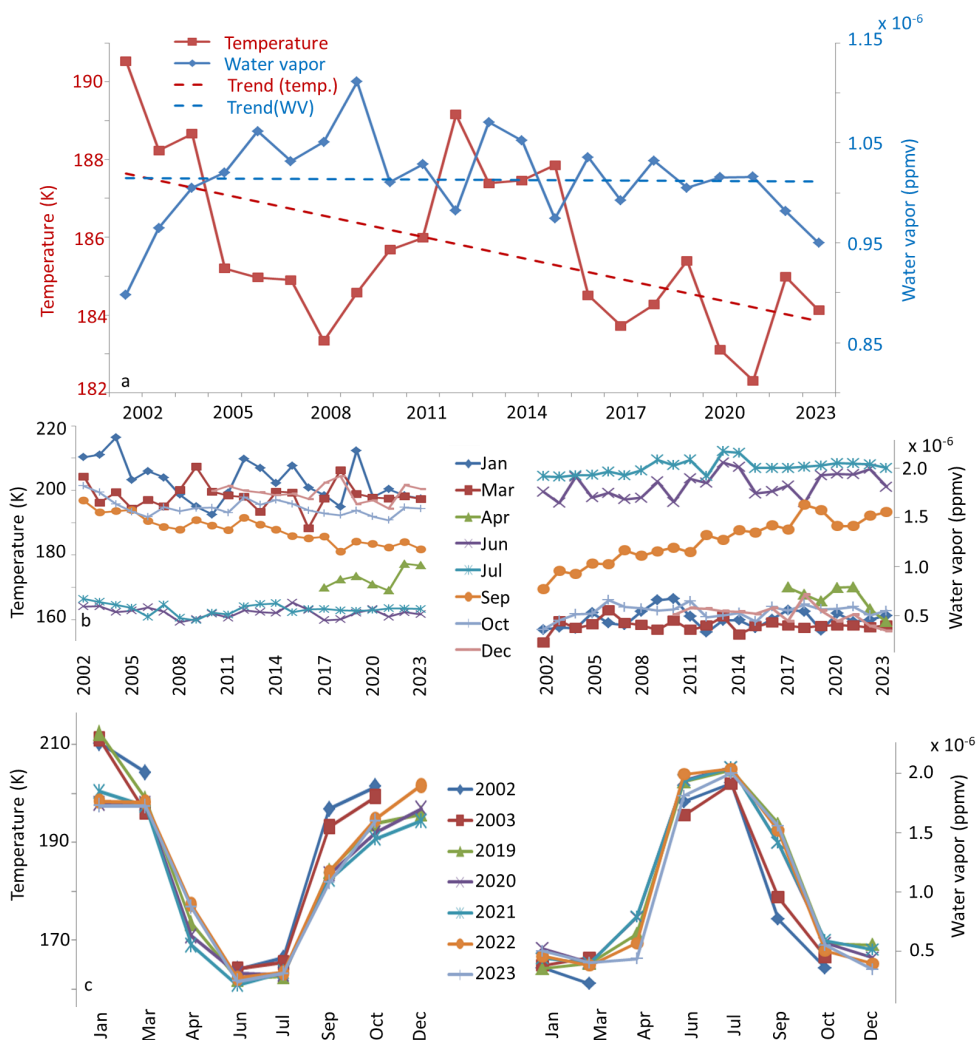
315 Figure 4. Temporal variation of temperature and water vapors over the equator

316 3.3 Temperature and water vapor variation over the North Pole

317 Monthly averaged temperature data for selected eight months data, 2002 (~190K) was the hottest, and  
 318 2023 (~182K) was the coldest year during the study period. June 2008 (~159K) was the coldest and  
 319 January 2002 (~210K) was the hottest month. Overall, there is a decreasing trend of temperature  
 320 (~4K/decade) in the North Pole of the mesopause region. This decreasing trend in temperature is more  
 321 prompt during September and less prompt during June and July. The monthly averaged temperature at  
 322 two equinoxes (Mar/Apr and Sep/Oct) were 185.57K and 191.50K respectively. Similarly, monthly  
 323 averaged temperatures at two solstices (Jun/July and Dec/Jan) were 162.64K and 201.14K  
 324 respectively, indicating the coldest temperature during June and July and the hottest temperature



325 during January and December throughout the whole study period. Our results are similar to those Xu  
326 et al., (2007) showed a warmer mesopause at high latitudes during the December solstice than  
327 it is in the June solstice. At high latitudes, the tendency term associated with vertical advection  
328 reaches a maximum of 0.7 ppmv/day at 70-85 km in NH (Chandra et al., 1997). Generally,  
329 temperature is not too much changing with altitude. The average temperature for all months  
330 is around  $200 \pm 10\text{K}$  in the mesopause region. June showed a completely different pattern  
331 than the other selected seven months. During June monthly temperature at 80km altitude was  
332 ( $\sim 160\text{K}$ ) and further decreased up to  $\sim 134\text{K}$  at 90 km altitude and then sharply increased  
333 ( $\sim 250\text{K}$ ) at the altitude of 100km. Average temperature during January was  $\sim 208 \pm 5\text{K}$  almost  
334 constant with increasing altitude and showed very little decrease ( $\sim 8\text{K}/20\text{Km}$ ) altitude in  
335 temperature. The temperature range during September was between 202-172K. There was a  
336 clear temperature decrease between 84 to 96km during September. The temperature during  
337 March showed a decreasing trend with increasing altitude. The average temperature at 80km  
338 during March was around 210K and decreased to  $\sim 185\text{K}$  at an altitude of 100km.



339

340 Figure 5 is the Same as Figure 4 but represents the North Pole

341 Monthly averaged WV data for selected eight months data, 2002 (~0.89ppmv) followed by 2023  
 342 (~0.95ppmv) were the two least content WV years, and 2009 (~1.11ppmv) followed by 2013  
 343 (~1.07ppmv) were the two maximum content of WV years during the study period (2002 – 2023). On  
 344 average July (~2.0ppmv) had the maximum WV content followed by June (~1.80ppmv) and March  
 345 (0.40ppmv) followed by January (0.47ppmv) had the minimum WV content. July 2013 (2.17) and  
 346 March 2002 (0.22) were the maximum and minimum WV content months during the study period.  
 347 There is no clear increasing/decreasing trend of WV over the selected space of the North Pole of the  
 348 mesopause region. Monthly averaged WV at two equinoxes (Mar/Apr and Sep/Oct) was 0.54 and  
 349 0.90ppmv respectively.





350 Similarly monthly averaged temperature at two solstices (Jun/July and Dec/Jan) were 1.90ppmv and  
351 0.49ppmv respectively, indicating relatively high WV content during June and July and low during  
352 December and January, this is because at middle and high latitudes, the general transport of H<sub>2</sub>O is  
353 directed upward in summer and downward in winter. Averaged WV content at lower altitudes 81, 82,  
354 and 83km were 2.98, 2.73, and 2.40ppmv respectively, and decreased with altitude in all selected  
355 months. As mentioned in section 2.2, SABER H<sub>2</sub>O is biased low by ~20% in polar summer above  
356 80 km. It means SABER H<sub>2</sub>O reflects the polar winter and spring descent very well but in the  
357 summer PMC region, the enhancement is weaker than expected. The decreasing trend in temperature  
358 is clear but there is no clear trend in WV 5a (yearly averaged). Monthly averaged variations in  
359 temperature and WV are shown in Figure 4b, having a clear inverse relation in selected months and  
360 years Figure 5c.

361

#### 362 3.4 Temperature and water vapor variation over the South Pole

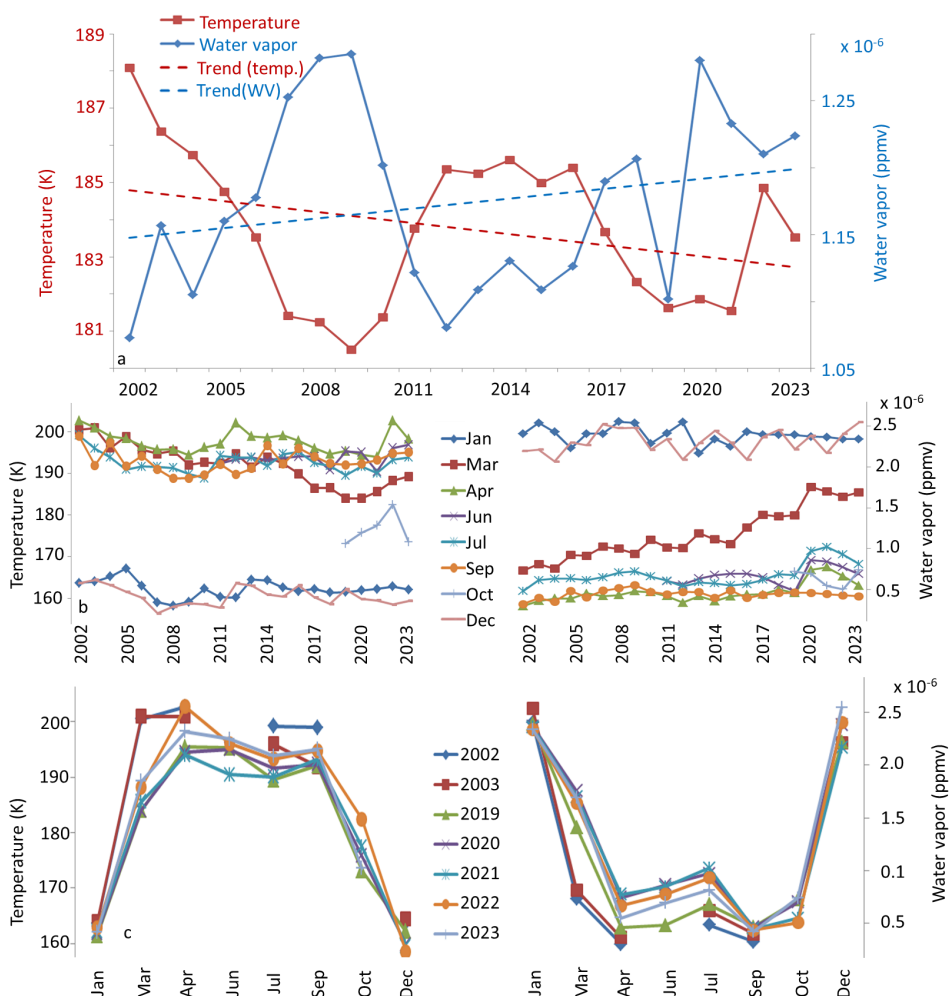
363 Based on the monthly averaged temperature data for selected eight months data, 2002 (~188K) was  
364 the hottest, and 2009 (~180K) was the coldest year during the study period. December 2007 (~156K)  
365 was the coldest and March 2003 (~201K) was the hottest month. Overall, there is a decreasing trend  
366 of temperature (~1.5K/decade) in the South Pole of the mesopause region. This decrease in  
367 temperature was relatively clearly visible in March. On average April (197.64K) followed by June  
368 and July were the hottest months and (December and January) were the coldest months throughout the  
369 study period. Temperatures in January and December were 10 to 15K lower than the other six selected  
370 months. The monthly averaged temperature at two equinoxes (Mar/Apr and Sep/Oct) were 194.85K  
371 and 184.69K respectively. Similarly, monthly averaged temperatures at two solstices (Jun/July and  
372 Dec/Jan) were 193.21K and 161.41K respectively, indicating the coldest temperature during January  
373 and December and the hottest temperature during March and April throughout the whole study period.  
374 Temperature variation with respect to altitude was different for January/December than for other  
375 selected months. During winter (January/December) temperature was first decreased up to 92 Km  
376 altitude and then increased to 93km and onward altitudes.

377

378 Monthly averaged WV data for selected eight months data, 2002 (~1.07ppmv) followed by 2012  
379 (~1.08ppmv) were the two least content WV years, and 2009 (~1.28ppmv) followed by 2008  
380 (~1.28ppmv) were the two maximum content of WV years during the study period (2002 – 2023). On  
381 average January (2.4 ppmv) had the maximum WV content followed by December (2.3 ppmv) and  
382 September (0.45 ppmv) followed by April (0.47 ppmv) has the minimum WV content (Figure 6).  
383 Overall, there is an increasing trend of WV (~0.08ppmv/decade) over the South Pole of the  
384 mesopause region. The monthly averaged WV at two equinoxes (Mar/Apr and Sep/Oct) was 0.82 and  
385 0.54ppmv lower than the monthly averaged temperature at two solstices (Jun/July and Dec/Jan) which



386 were 0.67ppmv and 2.3 ppmv respectively. This indicates relatively high WV content during winter  
 387 (December and January). In the SH temperature is colder at mid-to-high latitudes during January  
 388 (Wang et al., 2022), had relatively high WV content. At high latitudes, the tendency term associated  
 389 with vertical advection reaches a minimum of -0.35 ppmv/day in SH (Chandra et al., 1997). WV  
 390 content at lower altitudes 81, 82, and 83km were 3.25, 3.01, and 2.74ppmv respectively, and  
 391 decreased with altitude in all selected months. Temperature and WV trends and their interrelationship  
 392 are given in Figure 6.



393

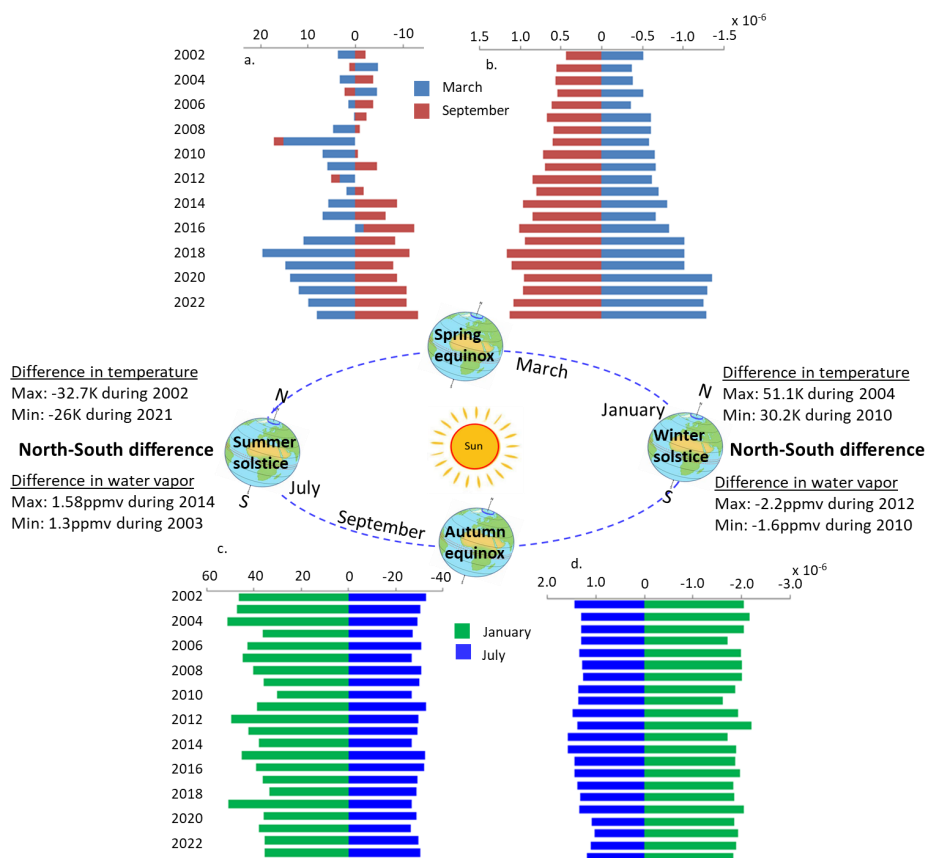
394 Figure 6. Same as Figure 4 but represents the South Pole region

395 4. Inter and intra-comparison at solstices, equinoxes, and Poles

396 The average temperature at the summer solstice (June and July) is 162.64K, which is 38.5K lower  
 397 than that of the winter solstice (December and January). Similarly, the average WV at summer



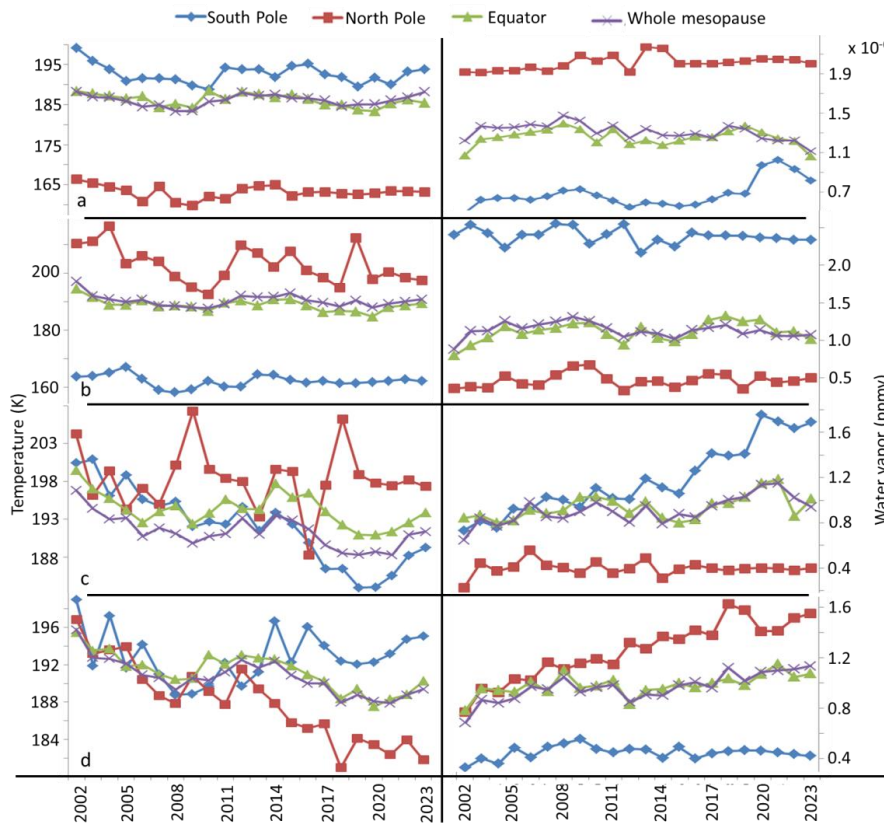
398 solstice is 1.92ppmv which is ~1.43ppmv greater than that of winter solstice. The difference between  
 399 the Noth-South poles temperature and WV at equinoxes and soloists is shown in Figure 7.



400

401 Figure 7. Difference in north-south temperature (a,c) and water vapor content (b,d) at two  
 402 equinoxes (March and September) and two solstices (January and July)

403 The difference between NH and SH temperature and WV at the solstice is higher than the difference  
 404 at the two equinoxes, indicating that the temperature and WV at both equinoxes are relatively close  
 405 however it look to increase in the future. The maximum and minimum difference in winter solstice  
 406 (January's) temperature (NH-SH) was during 2004 (51.11K) and 2010(30.24K) respectively, and in  
 407 summer solstice (July's) temperature (NH-SH) was during 2002 (-32.79K) and 2021(-26.60K)  
 408 respectively. Similarly, the maximum and minimum difference in July's WV (NH-SH) was during  
 409 2014(1.58ppmv) and 2003(1.3ppmv) respectively, and in January's WV (NH-SH) was during 2012 (-  
 410 2.2ppmv) and 2010(-1.60ppmv) respectively. For equinoxes WV and Temperature differences  
 411 between NH and SH are increasing with time, however, this difference for solstices is relatively  
 412 constant and has no increasing or decreasing trend with time.



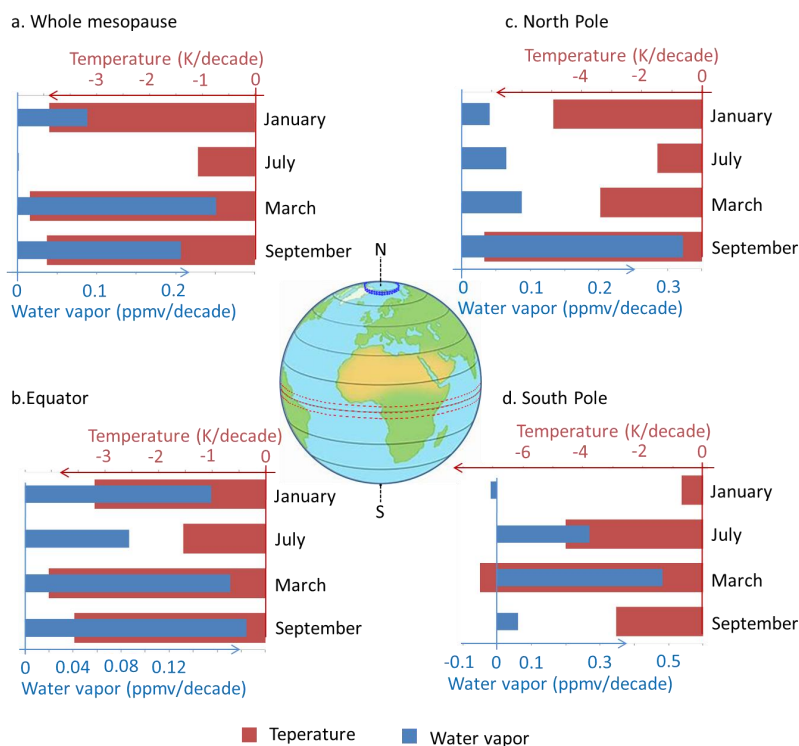
413

414 Figure 8. Intra-annual temperature and water vapor variations. The left column is for  
415 Temperature and the right column is for water vapor in selected months a. July, b. January, c.  
416 March, and d. September

417 The June and July temperature is colder at high latitudes (North Pole) in the summer hemisphere. In  
418 addition, at summer high latitudes (North Pole for July and South Pole for January), the mesopause  
419 temperature is ~5K colder. Examination of Figure 8 shows a clear temperature difference between  
420 summer mesopause temperatures in the two hemispheres, with the southern temperatures appearing to  
421 be at least a few K warmer during most of the summer season. The observed temperature differences  
422 are highly significant ranging from 156K during December (South Pole), to around 210 K during  
423 January (North Pole). The mean seasonal difference (the average of these values) is close to ~183K.  
424 The inter-hemispheric comparison showed a clear difference in Temperature and WV. The difference  
425 may be due to the reduced gravity waves and 50% weaker winds in the southern hemisphere  
426 measured by Vincent, (1994), resulting in reduced mesospheric circulation. The summer season  
427 ranges from May to August in the NH and from November to February in the SH, and is centered on  
428 the solstice (Huaman and Balsley, 1999).



429 This result is close to (Wang et al., 2022) and (Xu et al., 2007) who found that the mesopause during  
 430 the June solstice is colder than that during the December solstice. There is a slight difference in  
 431 magnitude may be due to the different lengths of the SABER temperature data set and using different  
 432 heights of the mesopause region. Xu et al., (2007) used initial 4 years of SABER data, and (Wang et  
 433 al., 2022) used 18 years of data set. Winter solstice (January) was the higher temperature month for  
 434 the North Pole and the lower temperature month South Pole (Figure 8). Similarly, the summer solstice  
 435 (July) was the higher temperature month for the South Pole and the lower temperature month North  
 436 Pole. A similar but lower temperature difference was also observed for two equinoxes (Figure 8 left  
 437 column). A clear inverse relation between temperature and WV is shown in Figure 8.



438

439 Figure 9. Temperature and water vapor trends for selected locations and months during the  
 440 study period.

441 At winter solstice (January), we observed less WV for the North Pole and relatively more WV for the  
 442 South Pole. Similarly, at the summer solstice (July) lower WV for the South Pole and more WV for  
 443 the North Pole. There is a relatively large difference in WV of winter solstice and summer solstices as  
 444 compared to the two equinoxes.

445 A decreasing trend in temperature and an increasing trend in WV in all selected locations (whole  
 446 mesopause, North Pole, South Pole, and the Equator) and selected months (January, July for solstices



447 and March, September for equinoxes) are shown in Figure 9. A cooling trend in temperature was also  
448 reported in the past such as  $-9.2$  K/decade in winter (Semenov, 2000),  $0.64$  K/decade (She et al.,  
449 2015);  $-5.0$ K/decade (Winter) (Golitsyn et al., 1996), and  $-0.075 \pm 0.043$  K/year (Zhao et al., 2020).  
450 Winter mesopause temperature trends ( $-6$  to  $-2$  K/decade) are generally stronger than summer ones  
451 ( $-2$  to  $+0.5$  K/decade (Offermann et al., 2010). A maximum decreasing trend in temperature and an  
452 increasing trend in WV is during March at the South Pole followed by September at the North Pole  
453 (Figure 9). A slight increase in WV at the South Pole was observed during January. In the summer  
454 hemisphere, the upwelling in high latitudes induces adiabatic cooling and creates a cold summer  
455 mesopause at high latitudes (Wang et al., 2022). Upwelling causes a strong adiabatic cooling in the  
456 summer mesosphere, affecting high latitudes. Therefore, at high latitudes in the summer hemisphere,  
457 this adiabatic cooling effect (induced by the upwelling of the mesospheric circulation) creates a cooler  
458 summer mesopause (Figure 9c). There is a strong upward transport by the mesospheric residual  
459 circulation in the summer high latitudes. On the other side, in the winter hemisphere, the upwelling of  
460 the lower thermosphere residual circulation causes cooling, and the downwelling of the mesospheric  
461 residual circulation causes warming.

462

## 463 5. Discussions

464 A variety of ground-based RADAR and LIDAR, satellite data, and model simulations (Table 1) have  
465 been examined in the mesopause region. However, a few studies showed a detailed spatial and  
466 temporal variation of temperature and WV. In this study, we presented the long-term differences in  
467 temperature, and WV between the two hemispheres, two solstices, and two equinoxes in selected  
468 months to gain a better understanding of spatial and temporal variation of temperature and WV at  
469 high altitude mesopause.

470 The mesopause temperature during 2002–2023 showed a cooling trend through all selected latitudes  
471 ranging from  $\sim 0.06$  to  $-0.4$  K/decade. Monthly averaged temperature data showed that 2002 was the  
472 hottest and 2018 was the coldest year during the study period. A decreasing trend in temperature was  
473 also reported by other authors in the past (Zhao et al., 2020 (Avg:  $-0.75$ K/decade); Dalin et al., 2020  
474 ( $-2.4$ K/decade); Yuan et al., 2019 ( $\sim -2.4$ K/decade); French et al., 2020( $-1.2$ K/decade)). Similarly,  
475 Mlynczak et al., (2022) found significant cooling and contraction from 2002 to 2019 due to a weaker  
476 solar cycle. According to Zhao et al., (2020), the cooling trends in the SH are stronger than those in  
477 the NH. At the same time (Dalin et al., 2020) showed relatively stronger cooling at the summer  
478 mesopause ( $-2.4$ K/decade), than that of winter mesopause ( $-0.4$  K/decade). Our results showed a  
479 significant cooling trend of  $\sim 4$ K/decade at the North Pole and a relatively low cooling trend  
480 ( $\sim 1.5$ K/decade) at the South Pole. The difference in results may be due to the difference in temporal  
481 and spatial datasets. Seasonal temperature variations at the mesopause region are distinct, with a  
482 summer minimum (June  $\sim 180$ K, July  $\sim 183$ K) and a winter maximum (January  $\sim 197$ K, December



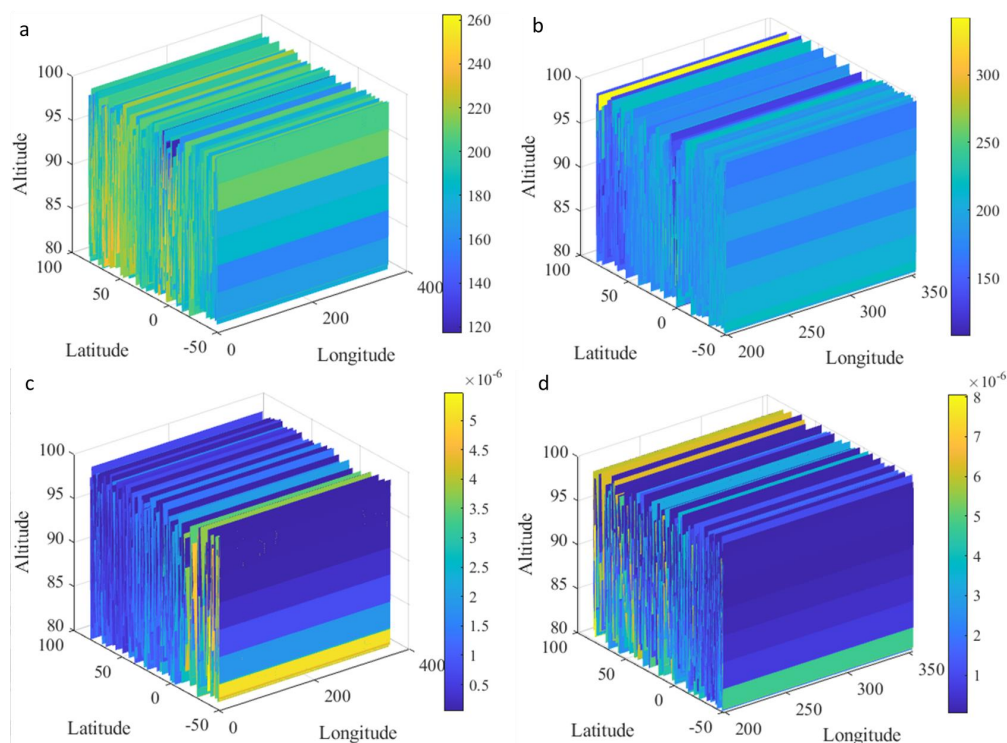
483 ~190K). The monthly averaged temperatures at two solstices (Jun/July and Dec/Jan) were 184.55K  
484 and 188.20K respectively, indicating the coldest temperature during June and July throughout the  
485 whole study period. Mesopause during the summer (June and July) solstice is ~ 3.65K colder than that  
486 during the winter (December and January) solstice.

487 A clear hemispheric asymmetry in temperature (Figure 7) was observed, possibly related to solar  
488 forcing and gravity wave forcing further discussed in (Xu et al., 2007). The mesopause temperature  
489 varies from (Min: 182.3K, Max: 190.5K, Avg: 185.7K) in the summer polar region to (Min: 180.5K,  
490 Max: 188.1K, Avg: 183.7K) in the winter polar region. Summer solstice was relatively colder  
491 (~184K) than winter solstice (188K) for the whole mesopause case. Xu et al., (2007) showed a  
492 warmer winter mesopause (~190K) than that of summer mesopause (~126K). In addition, at summer  
493 high latitudes mesopause temperature (the North Pole for June/July) is 1.23K warmer than the South  
494 Pole or December/January. At winter solstice (December and January), the North Pole's temperature  
495 is higher than the South Pole's temperature and has relatively low WV content. At summer solstice  
496 (June and July), the South Poles's temperature is higher than the North Pole Temperature. Wang et  
497 al., (2022); Xu et al., (2007) found that the mesopause during the June solstice is ~6–9 K colder than  
498 that during the December solstice. Huaman and Balsley, 1999 showed a predominant warmer SH (by  
499 6K) around the summer solstice at 64° latitude for a limited period (selected months of 1994),  
500 measuring the temperature at different months in the two hemispheres. The slight difference in results  
501 may be due to the different lengths of the SABER temperature data set and using different heights of  
502 the mesopause region. We used a constant altitude of 80 to 100km during all seasons and latitudes can  
503 change the results presented in this study than other studies in the past. The mesopause is ~1 km  
504 higher at most latitudes and relatively warmer at middle to high latitudes in winter (around December  
505 solstice) than it is in summer (around June solstice). At the equator, the mesopause is at a higher  
506 altitude for all seasons. During the equinox months, the mesopause is at a constant altitude and  
507 becomes discontinuous at the middle latitudes in the summer hemisphere from the equinoxes to the  
508 solstices (Wang et al., 2022). Temporal and spatial variation of mesopause height is discussed by Xu  
509 et al., (2007); Wang et al., (2022). The monthly averaged temperature at two equinoxes (Mar/Apr and  
510 Sep/Oct) was 191.66K and 191.16K respectively indicating almost similar temperatures.

511 The adiabatic cooling effects are stronger due to stronger vertical wind at high latitudes and resulting  
512 in a lower mesopause temperature and altitude (Wang et al., 2022). These adiabatic cooling effects are  
513 strong enough to affect the mesopause altitude even during the transitional months between the  
514 solstices and the equinoxes. Upwelling causes a strong adiabatic cooling in the summer mesosphere,  
515 affecting high latitudes. Therefore, at high latitudes in the summer hemisphere, this adiabatic cooling  
516 effect (induced by the upwelling of the mesospheric circulation) creates a cooler summer mesopause.  
517 There is also a strong upward transport by the mesospheric residual circulation in the summer high  
518 latitudes. On the other side, in the winter hemisphere, the upwelling of the lower thermosphere  
519 residual circulation causes cooling, and the downwelling of the mesospheric residual circulation



520 causes warming. An increase in CO<sub>2</sub> was correlated with the decrease in temperature, which is one of  
521 the possible reasons for the temperature-decreasing trend. CO<sub>2</sub> is transported from low altitudes and  
522 affects the infrared cooling rate leading to globally warmer mesopause temperatures (Chabrillat et al.,  
523 2002) and enhanced differences between the summer and winter temperatures (Smith, 2004). More  
524 detailed analyses (of the energy budget, the response of nonmigrating tides, gravity waves,  
525 geomagnetic activities, etc.) are required for further improvements.  
526 WV measurements showed a decadal cycle (2002-2011, and 2011-2023) that was anti-correlated with  
527 temperature variability and showed relatively more WV during solar minimum. A similar  
528 anticorrelated relation between WV and solar variability was observed by (Hervig and Siskind, 2006),  
529 and showed ~25% more WV during solar minimum. Anticorrelated relation between WV is also  
530 shown by (Yue et al., 2019; Dalin et al., 2023). We find a maximum WV mixing ratio in June and  
531 July and a higher annual variability than at the equator. At the polar summer mesopause, the WV  
532 mixing ratio sharply rises from the beginning of May up to mid-September. The summer maximum  
533 (North Pole) is a more isolated feature than at the equator: it has a rather sharp increase in WV in  
534 April and a fast decline in autumn (September/October). Three-dimensional variations of temperature  
535 and WV for January 2002 and July 2015 are shown in Figure 10.



536

537 Figure 10. Three-dimensional variation of temperature and water vapor in selected months  
538 a,c) January 2002 and b,d) July 2015 for the North Pole region.





539 A comparison of temperature and water vapor among the North Pole, South Pole, and Equator is  
 540 shown in Table 2.

541 Table 2. Comparison of temperature and water vapor among North Pole, South Pole, and  
 542 Equator

		North Pole		South Pole		Equator	
		Maximum	Minimum	Maximum	Minimum	Maximum	Minimum
Temperature	Yearly	2002 (190K)	2023 (182K)	2002(188K)	2009(180K)	2002(194K)	2019(188K)
	Monthly	Jan -2002 (210K)	Jun-2008 (159K)	Mar-2003(201K)	Dec-2007(156K)	Mar-2014(198K)	Jun-2009(183K)
	Trend	Cooling trend ~4K/decade		Cooling trend ~1.5K/decade		Cooling trend ~1.5K/decade	
	Order	DJ(201K)>SO(191.5K)>MA(185.5K)>JJ(162.6K)		MA(194K)>JJ(193K)>SO(184K)>DJ(161K)		MA(194K)>SO(192K)>DJ(189K)>JJ(185K)	
	Altitude	100km(282.7K)	90km(125.3K)	100km(261.1K)	91km(134.1K)	85km(215.6K)	98km(171.9K)
Water vapor	Yearly	2009(1.11ppmv)	2002(0.89ppmv)	2009(1.28ppmv)	2002(1.07ppmv)	2009(1.12ppmv)	2002(0.88ppmv)
	Monthly	July-2015(2.0ppmv)	Mar-2023(0.4ppmv)	Jan-2016(2.4ppmv)	Apr-2002(0.30ppmv)	July-2008(1.39ppmv)	Oct-2023(0.74ppmv)
	Trend	Increasing trend ~0.06ppmv/decade		Increasing trend ~0.08ppmv/decade		Increasing trend ~0.09ppmv/decade	
	Order	JJ(1.90)>SO(0.9)>MA(0.54)>DJ(0.49) in ppmv		DJ(2.3)>MA(0.82)>JJ(0.67)>SO(0.45) in ppmv		JJ(1.19)>DJ(1.08)>MA(0.9)=SO(0.9) in ppmv	
	Altitude	80km(7.18ppmv)	100km(0.05ppmv)	80km(7.34ppmv)	100km(0.03ppmv)	80km(4.14ppmv)	100km(0.03ppmv)

543

544 MA: March April averaged (spring equinox)

545 SO: September October averaged (autumn equinox)

546 JJ: June July averaged (summer solstice)

547 DJ: December January averaged (winter solstice)

548



549        6. Conclusions

550    In the present study, we used TIMED/SABER long-term monthly temperature and WV data to  
551    analyze the spatial and temporal distribution of the mesopause temperature and WV in selected  
552    timings and locations. The results indicate high spatial and temporal variation in temperature and had  
553    an inverse correlation with WV. Yearly averaged temperature for selected eight months of data, 2002  
554    was the hottest (~193K) followed by 2003 (191K) and 2018 was the coldest (~187K) year followed  
555    by 2008 (187.1K) during the study period (2002 – 2023). Seasonal temperature variations at the  
556    mesopause region are distinct, with a summer minimum (June ~ 180K, July ~183K) and a winter  
557    maximum (January ~197K, December ~190K). The monthly averaged temperature at two solstices  
558    (Jun/July and December/January) were 184.55K and 188.20K respectively, indicating the coldest  
559    temperature during June and July throughout the whole study period. Mesopause during the summer  
560    (June and July) solstice is ~ 3.65K colder than that during the winter (December and January) solstice.  
561    A cooling trend was observed during twenty-two years of monthly observations. The cooling trends at  
562    high latitudes (North Pole) are relatively stronger than those at the Equator and South Pole. The  
563    mesopause temperature is colder in summer than in winter. Air is drawn downward in winter and  
564    upward in summer keeping away mesopause from thermodynamic equilibrium creating very low  
565    temperatures in summer (June and July) and relatively high temperatures in winter (January and  
566    December). The north-south temperature difference was maximum during the winter solstice of 2004.  
567    The vertical temperature gradient per km lies between -1.74 and 2.43 K during January, -2.14 and  
568    1.28 K during March, -2 and 1.7 during April, -2 and 4.5 during June, -1.64 and 3.54 during July, -  
569    1.88 and 1.22 during September, -1.83 and 1.22K during October and -2.27 and 3.94K during  
570    December in the 80 to 100km altitude region, with values increasing in general with altitude and  
571    toward the summer pole (Schubert et al., 1990).

572    Based on the monthly averaged WV for selected eight months of data, 2018 had a relatively higher  
573    amount of water content (~1.14ppmv) followed by 2008 (1.14ppmv), and 2002 has the least amount  
574    of WV (~0.89ppmv) year followed by 2014 and 2003 (~1.0 ppmv) during the study period (2002 –  
575    2023). July 2015 and January 2016 had maximum WV content at the summer and winter poles  
576    respectively. Overall there is an increasing WV trend in all selected locations. The north-south  
577    difference in WV was maximum during the winter solstice of 2012. The North Pole was coldest  
578    during the summer solstice and had a relatively large amount of water content. Upward transport,  
579    solar-cycle-induced variations in Lyman- $\alpha$  radiation, methane oxidation, and vertical advection are  
580    the responsible factors for changing WV content in the mesopause region. The possible loss of WV  
581    in the region is by photolysis and diffusion. We find that the occurrence of a WV maximum coincides  
582    with the temperature minimum in both hemispheres.

583

584



585 Author contributions

586 CG and SK initiated the idea; CG and DG performed the measurements and required calculations;  
587 CG, DG and YY wrote the manuscript draft; SK and XG reviewed and edited the manuscript.

588 Competing interests

589 The authors declare that they have no conflict of interest.

590 Acknowledgments

591 The study was supported by the role of land air system in the arctic tropical correlation, National key  
592 research and development plan (2022YFF0801703) and the State Key Laboratory of Cryosphere  
593 Sciences (SKLCS20 ZZ-2022). We thank Faiza Gul for her encouragement and motivation. We  
594 acknowledge NASA and supporting departments for the development of the SABER and TIMED  
595 mission. Thanks to Global Atmospheric Technologies & Sciences (GATS) for providing data on  
596 temperature and water vapor. We are grateful to the SABER retrieval team from GATS, Inc. for their  
597 tireless effort to produce the SABER temperature and H<sub>2</sub>O data.

598

599 References

- 600 Ammosov, P., Gavriyeva, G., Ammosova, A., and Koltovskoi, I.: Response of the mesopause  
601 temperatures to solar activity over Yakutia in 1999–2013, *Adv. Sp. Res.*, 54, 2518–2524, 2014.
- 602 Arnold, F. and Krankowsky, D.: Ion composition and electron-and ion-loss processes in the Earth's  
603 atmosphere, in: *Dynamical and Chemical Coupling Between the Neutral and Ionized Atmosphere:*  
604 *Proceedings of the NATO Advanced Study Institute held at Spåtind, Norway, April 12–22, 1977*, 93–  
605 127, 1977.
- 606 Beig, G.: Long-term trends in the temperature of the mesosphere/lower thermosphere region: 1.  
607 Anthropogenic influences, *J. Geophys. Res. Sp. Phys.*, 116, 2011a.
- 608 Beig, G.: Long-term trends in the temperature of the mesosphere/lower thermosphere region: 2. Solar  
609 response, *J. Geophys. Res. Sp. Phys.*, 116, 2011b.
- 610 Beig, G., Keckhut, P., Lowe, R. P., Roble, R. G., Mlynczak, M. G., Scheer, J., Fomichev, V. I.,  
611 Offermann, D., French, W. J. R., and Shepherd, M. G.: Review of mesospheric temperature trends,  
612 *Rev. Geophys.*, 41, 2003.
- 613 Berger, U. and Lübken, F.: Mesospheric temperature trends at mid-latitudes in summer, *Geophys.*  
614 *Res. Lett.*, 38, 2011.
- 615 Berger, U. and Von Zahn, U.: The two-level structure of the mesopause: A model study, *J. Geophys.*  
616 *Res. Atmos.*, 104, 22083–22093, 1999.
- 617 Berger, U. and Von Zahn, U.: Icy particles in the summer mesopause region: Three-dimensional  
618 modeling of their environment and two-dimensional modeling of their transport, *J. Geophys. Res. Sp.*  
619 *Phys.*, 107, SIA-10, 2002.
- 620 Bevilacqua, R. M., Olivero, J. J., Schwartz, P. R., Gibbins, C. J., Bologna, J. M., and Thacker, D. J.:  
621 An observational study of water vapor in the mid-latitude mesosphere using ground-based microwave  
622 techniques, *J. Geophys. Res. Ocean.*, 88, 8523–8534, 1983.
- 623 Bittner, M., Offermann, D., and Graef, H. H.: Mesopause temperature variability above a midlatitude



- 624 station in Europe, *J. Geophys. Res. Atmos.*, 105, 2045–2058, 2000.
- 625 Brasseur, G. and Solomon, S.: *Aeronomy of the Middle Atmosphere*, 452 pp., D, 1986.
- 626 Brasseur, G. P. and Solomon, S.: *Aeronomy of the middle atmosphere: Chemistry and physics of the*  
627 *stratosphere and mesosphere*, Springer Science & Business Media, 2005.
- 628 Chabrilat, S., Kockarts, G., Fonteyn, D., and Brasseur, G.: Impact of molecular diffusion on the CO<sub>2</sub>  
629 distribution and the temperature in the mesosphere, *Geophys. Res. Lett.*, 29, 11–19, 2002.
- 630 Chandra, S., Jackman, C. H., Fleming, E. L., and Russell III, J. M.: The seasonal and long term  
631 changes in mesospheric water vapor, *Geophys. Res. Lett.*, 24, 639–642, 1997.
- 632 Chu, X., Gardner, C. S., and Roble, R. G.: Lidar studies of interannual, seasonal, and diurnal  
633 variations of polar mesospheric clouds at the South Pole, *J. Geophys. Res. Atmos.*, 108, 2003.
- 634 Clancy, R. T. and Rusch, D. W.: Climatology and trends of mesospheric (58–90 km) temperatures  
635 based upon 1982–1986 SME limb scattering profiles, *J. Geophys. Res. Atmos.*, 94, 3377–3393, 1989.
- 636 Dalin, P., Kirkwood, S., Pertsev, N., and Perminov, V.: Influence of solar and lunar tides on the  
637 mesopause region as observed in polar mesosphere summer echoes characteristics, *J. Geophys. Res.*  
638 *Atmos.*, 122, 10–369, 2017.
- 639 Dalin, P., Perminov, V., Pertsev, N., and Romejko, V.: Updated long-term trends in mesopause  
640 temperature, airglow emissions, and noctilucent clouds, *J. Geophys. Res. Atmos.*, 125,  
641 e2019JD030814, 2020.
- 642 Dalin, P., Suzuki, H., Pertsev, N., Perminov, V., Shevchuk, N., Tsimerinov, E., Zalcik, M., Brausch,  
643 J., McEwan, T., and McEachran, I.: The strong activity of noctilucent clouds at middle latitudes in  
644 2020, *Polar Sci.*, 35, 100920, 2023.
- 645 Dessler, A. E., Schoeberl, M. R., Wang, T., Davis, S. M., Rosenlof, K. H., and Vernier, J.: Variations  
646 of stratospheric water vapor over the past three decades, *J. Geophys. Res. Atmos.*, 119, 12–588, 2014.
- 647 Dopplack, T. G.: Radiative heating of the global atmosphere, *J. Atmos. Sci.*, 29, 1278–1294, 1972.
- 648 Dyrland, M. E., Mulligan, F. J., Hall, C. M., Sigernes, F., Tsutsumi, M., and Deehr, C. S.: Response  
649 of OH airglow temperatures to neutral air dynamics at 78 N, 16 E during the anomalous 2003–2004  
650 winter, *J. Geophys. Res. Atmos.*, 115, 2010.
- 651 Esplin, R., Mlynczak, M. G., Russell, J., Gordley, L., and Team, S.: Sounding of the Atmosphere  
652 using Broadband Emission Radiometry (SABER): Instrument and science measurement description,  
653 *Earth Sp. Sci.*, 10, e2023EA002999, 2023.
- 654 Fiedler, J., Baumgarten, G., Berger, U., Hoffmann, P., Kaifler, N., and Lübken, F.-J.: NLC and the  
655 background atmosphere above ALOMAR, *Atmos. Chem. Phys.*, 11, 5701–5717, 2011.
- 656 French, W. J. R., Mulligan, F. J., and Klekociuk, A. R.: Analysis of 24 years of mesopause region OH  
657 rotational temperature observations at Davis, Antarctica–Part 1: long-term trends, *Atmos. Chem.*  
658 *Phys.*, 20, 6379–6394, 2020a.
- 659 French, W. J. R., Klekociuk, A. R., and Mulligan, F. J.: Analysis of 24 years of mesopause region OH  
660 rotational temperature observations at Davis, Antarctica–Part 2: Evidence of a quasi-quadrennial  
661 oscillation (QQO) in the polar mesosphere, *Atmos. Chem. Phys.*, 20, 8691–8708, 2020b.
- 662 Fueglistaler, S. and Haynes, P. H.: Control of interannual and longer-term variability of stratospheric  
663 water vapor, *J. Geophys. Res. Atmos.*, 110, 2005.



- 664 Golitsyn, G. S., Semenov, A. I., Shefov, N. N., Fishkova, L. M., Lysenko, E. V., and Perov, S. P.:  
665 Long-term temperature trends in the middle and upper atmosphere, *Geophys. Res. Lett.*, 23, 1741–  
666 1744, 1996.
- 667 Grygalashvyly, M., Sonnemann, G. R., Lübken, F., Hartogh, P., and Berger, U.: Hydroxyl layer:  
668 Mean state and trends at midlatitudes, *J. Geophys. Res. Atmos.*, 119, 12–391, 2014.
- 669 Gumbel, J., Siskind, D. E., Witt, G., Torkar, K. M., and Friedrich, M.: Influences of ice particles on  
670 the ion chemistry of the polar summer mesosphere, *J. Geophys. Res. Atmos.*, 108, 2003.
- 671 Hedin, A. E.: Extension of the MSIS thermosphere model into the middle and lower atmosphere, *J.*  
672 *Geophys. Res. Sp. Phys.*, 96, 1159–1172, 1991.
- 673 Hervig, M. and Siskind, D.: Decadal and inter-hemispheric variability in polar mesospheric clouds,  
674 water vapor, and temperature, *J. Atmos. solar-terrestrial Phys.*, 68, 30–41, 2006.
- 675 Hervig, M., McHugh, M., and Summers, M. E.: Water vapor enhancement in the polar summer  
676 mesosphere and its relationship to polar mesospheric clouds, *Geophys. Res. Lett.*, 30, 2003.
- 677 Hervig, M. E., Stevens, M. H., Gordley, L. L., Deaver, L. E., Russell III, J. M., and Bailey, S. M.:  
678 Relationships between polar mesospheric clouds, temperature, and water vapor from Solar  
679 Occultation for Ice Experiment (SOFIE) observations, *J. Geophys. Res. Atmos.*, 114, 2009.
- 680 Hervig, M. E., Siskind, D. E., Bailey, S. M., and Russell III, J. M.: The influence of PMCs on water  
681 vapor and drivers behind PMC variability from SOFIE observations, *J. Atmos. Solar-Terrestrial*  
682 *Phys.*, 132, 124–134, 2015.
- 683 Hervig, M. E., Berger, U., and Siskind, D. E.: Decadal variability in PMCs and implications for  
684 changing temperature and water vapor in the upper mesosphere, *J. Geophys. Res. Atmos.*, 121, 2383–  
685 2392, 2016.
- 686 Huaman, M. M. and Balsley, B. B.: Differences in near-mesopause summer winds, temperatures, and  
687 water vapor at northern and southern latitudes as possible causal factors for inter-hemispheric PMSE  
688 differences, *Geophys. Res. Lett.*, 26, 1529–1532, 1999.
- 689 Hurst, D. F., Oltmans, S. J., Vömel, H., Rosenlof, K. H., Davis, S. M., Ray, E. A., Hall, E. G., and  
690 Jordan, A. F.: Stratospheric water vapor trends over Boulder, Colorado: Analysis of the 30 year  
691 Boulder record, *J. Geophys. Res. Atmos.*, 116, 2011.
- 692 Jarvis, M. J.: Bridging the atmospheric divide, *Science (80-. )*, 293, 2218–2219, 2001.
- 693 Jensen, E. J. and Thomas, G. E.: Numerical simulations of the effects of gravity waves on noctilucent  
694 clouds, *J. Geophys. Res. Atmos.*, 99, 3421–3430, 1994.
- 695 Kalicinsky, C., Knieling, P., Koppmann, R., Offermann, D., Steinbrecht, W., and Wintel, J.: Long-  
696 term dynamics of OH\* temperatures over central Europe: trends and solar correlations, *Atmos. Chem.*  
697 *Phys.*, 16, 15033–15047, 2016.
- 698 Körner, U. and Sonnemann, G. R.: Global three-dimensional modeling of the water vapor  
699 concentration of the mesosphere-mesopause region and implications with respect to the noctilucent  
700 cloud region, *J. Geophys. Res. Atmos.*, 106, 9639–9651, 2001.
- 701 Kuhn, W. R. and London, J.: Infrared radiative cooling in the middle atmosphere (30–110 km), *J.*  
702 *Atmos. Sci.*, 26, 189–204, 1969.
- 703 López-Puertas, M., López-Valverde, M. A., Rinsland, C. P., and Gunson, M. R.: Analysis of the upper  
704 atmosphere CO<sub>2</sub> (ν<sub>2</sub>) vibrational temperatures retrieved from ATMOS/Spacelab 3 observations, *J.*  
705 *Geophys. Res. Atmos.*, 97, 20469–20478, 1992.



- 706 Lübken, F.-J., Rapp, M., and Strelnikova, I.: The sensitivity of mesospheric ice layers to atmospheric  
707 background temperatures and water vapor, *Adv. Sp. Res.*, 40, 794–801, 2007.
- 708 Lübken, F., Berger, U., and Baumgarten, G.: Stratospheric and solar cycle effects on long-term  
709 variability of mesospheric ice clouds, *J. Geophys. Res. Atmos.*, 114, 2009.
- 710 Lübken, F., Berger, U., and Baumgarten, G.: On the anthropogenic impact on long-term evolution of  
711 noctilucent clouds, *Geophys. Res. Lett.*, 45, 6681–6689, 2018.
- 712 Lübken, F. J.: Thermal structure of the mesopause region at polar latitudes, *J. Geophys. Res.*, 96,  
713 20841–20857, 1991.
- 714 Lübken, F. J., Zeche, M., Hoffner, J., and Rottger, J.: Temperatures, polar mesosphere summer  
715 echoes, and noctilucent clouds over Spitsbergen (78 degrees N), *J. Geophys. Res.*, 109, 2004.
- 716 Medvedeva, I. V and Ratovsky, K. G.: Multi-Year Variations in Temperature in Mesopause Region  
717 and F2-Region Peak Electron Density over Eastern Siberia, *Atmosphere (Basel)*, 14, 391, 2023.
- 718 Mlynczak, M. G.: Energetics of the mesosphere and lower thermosphere and the SABER experiment,  
719 *Adv. Sp. Res.*, 20, 1177–1183, 1997.
- 720 Mlynczak, M. G., Hunt, L. A., Garcia, R. R., Harvey, V. L., Marshall, B. T., Yue, J., Mertens, C. J.,  
721 and Russell III, J. M.: Cooling and contraction of the mesosphere and lower thermosphere from 2002  
722 to 2021, *J. Geophys. Res. Atmos.*, 127, e2022JD036767, 2022.
- 723 Mulligan, F. J., Horgan, D. F., Galligan, J. G., and Griffin, E. M.: Mesopause temperatures and  
724 integrated band brightnesses calculated from airglow OH emissions recorded at Maynooth (53.2 N,  
725 6.4 W) during 1993, *J. Atmos. Terr. Phys.*, 57, 1623–1637, 1995.
- 726 Murray, B. J. and Jensen, E. J.: Homogeneous nucleation of amorphous solid water particles in the  
727 upper mesosphere, *J. Atmos. solar-terrestrial Phys.*, 72, 51–61, 2010.
- 728 Nedoluha, G. E., Bevilacqua, R. M., Gomez, R. M., Siskind, D. E., Hicks, B. C., Russell III, J. M.,  
729 and Connor, B. J.: Increases in middle atmospheric water vapor as observed by the Halogen  
730 Occultation Experiment and the ground-based Water Vapor Millimeter-wave Spectrometer from 1991  
731 to 1997, *J. Geophys. Res. Atmos.*, 103, 3531–3543, 1998.
- 732 Nedoluha, G. E., Gomez, R. M., Hicks, B. C., Wrotny, J. E., Boone, C., and Lambert, A.: Water vapor  
733 measurements in the mesosphere from Mauna Loa over solar cycle 23, *J. Geophys. Res. Atmos.*, 114,  
734 2009.
- 735 Nedoluha, G. E., Michael Gomez, R., Allen, D. R., Lambert, A., Boone, C., and Stiller, G.: Variations  
736 in middle atmospheric water vapor from 2004 to 2013, *J. Geophys. Res. Atmos.*, 118, 11–285, 2013.
- 737 Nedoluha, G. E., Gomez, R. M., Boyd, I., Neal, H., Allen, D. R., Siskind, D. E., Lambert, A., and  
738 Livesey, N. J.: Measurements of mesospheric water vapor from 1992 to 2021 at three stations from  
739 the Network for the Detection of Atmospheric Composition Change, *J. Geophys. Res. Atmos.*, 127,  
740 e2022JD037227, 2022.
- 741 Noll, S., Kimeswenger, S., Proxauf, B., Unterguggenberger, S., Kausch, W., and Jones, A. M.: 15  
742 years of VLT/UVES OH intensities and temperatures in comparison with TIMED/SABER data, *J.*  
743 *Atmos. Solar-Terrestrial Phys.*, 163, 54–69, 2017.
- 744 Offermann, D., Donner, M., Knieling, P., Hamilton, K., Menzel, A., Naujokat, B., and Winkler, P.:  
745 Indications of long-term changes in middle atmosphere transports, *Adv. Sp. Res.*, 32, 1675–1684,  
746 2003.
- 747 Offermann, D., Donner, M., Knieling, P., and Naujokat, B.: Middle atmosphere temperature changes



- 748 and the duration of summer, *J. Atmos. solar-terrestrial Phys.*, 66, 437–450, 2004.
- 749 Offermann, D., Gusev, O., Donner, M., Forbes, J. M., Hagan, M., Mlynczak, M. G., Oberheide, J.,  
750 Preusse, P., Schmidt, H., and Russell III, J. M.: Relative intensities of middle atmosphere waves, *J.*  
751 *Geophys. Res. Atmos.*, 114, 2009.
- 752 Offermann, D., Hoffmann, P., Knieling, P., Koppmann, R., Oberheide, J., and Steinbrecht, W.: Long-  
753 term trends and solar cycle variations of mesospheric temperature and dynamics, *J. Geophys. Res.*  
754 *Atmos.*, 115, 2010.
- 755 Offermann, D., Wintel, J., Kalicinsky, C., Knieling, P., Koppmann, R., and Steinbrecht, W.: Long-  
756 term development of short-period gravity waves in middle Europe, *J. Geophys. Res. Atmos.*, 116,  
757 2011.
- 758 Oltmans, S. J. and Hofmann, D. J.: Increase in lower-stratospheric water vapour at a mid-latitude  
759 Northern Hemisphere site from 1981 to 1994, *Nature*, 374, 146–149, 1995.
- 760 Oltmans, S. J., Vömel, H., Hofmann, D. J., Rosenlof, K. H., and Kley, D.: The increase in  
761 stratospheric water vapor from balloonborne, frostpoint hygrometer measurements at Washington,  
762 DC, and Boulder, Colorado, *Geophys. Res. Lett.*, 27, 3453–3456, 2000.
- 763 Ortland, D. A., Hays, P. B., Skinner, W. R., and Yee, J.: Remote sensing of mesospheric temperature  
764 and O<sub>2</sub> ( $1\Sigma$ ) band volume emission rates with the high-resolution Doppler imager, *J. Geophys. Res.*  
765 *Atmos.*, 103, 1821–1835, 1998.
- 766 Pancheva, D., Mukhtarov, P., and Smith, A. K.: Climatology of the migrating terdiurnal tide (TW3) in  
767 SABER/TIMED temperatures, *J. Geophys. Res. Sp. Phys.*, 118, 1755–1767, 2013.
- 768 Perminov, V. I., Semenov, A. I., Medvedeva, I. V., and Pertsev, N. N.: Temperature variations in the  
769 mesopause region according to the hydroxyl-emission observations at midlatitudes, *Geomagn. Aeron.*,  
770 54, 230–239, 2014.
- 771 Petelina, S. V and Zsetsky, A. Y.: Temperature of mesospheric ice retrieved from the O-H stretch  
772 band, *Geophys. Res. Lett.*, 36, 2009.
- 773 Peter, R.: Stratospheric and mesospheric latitudinal water vapor distributions obtained by an airborne  
774 millimeter-wave spectrometer, *J. Geophys. Res. Atmos.*, 103, 16275–16290, 1998.
- 775 Remsberg, E., Damadeo, R., Natarajan, M., and Bhatt, P.: Observed responses of mesospheric water  
776 vapor to solar cycle and dynamical forcings, *J. Geophys. Res. Atmos.*, 123, 3830–3843, 2018.
- 777 Rogers, J. W., Stair Jr, A. T., Degges, T. C., Wyatt, C. L., and Baker, D. J.: Rocketborne measurement  
778 of mesospheric H<sub>2</sub>O in the auroral zone, *Geophys. Res. Lett.*, 4, 366–368, 1977.
- 779 Rong, P., Russell III, J. M., Marshall, B. T., Gordley, L. L., Mlynczak, M. G., and Walker, K. A.:  
780 Validation of water vapor measured by SABER on the TIMED satellite, *J. Atmos. Solar-Terrestrial*  
781 *Phys.*, 194, 105099, 2019.
- 782 Russell III, J. M., Gordley, L. L., Park, J. H., Drayson, S. R., Hesketh, W. D., Cicerone, R. J., Tuck,  
783 A. F., Frederick, J. E., Harries, J. E., and Crutzen, P. J.: The halogen occultation experiment, *J.*  
784 *Geophys. Res. Atmos.*, 98, 10777–10797, 1993.
- 785 Russell III, J. M., Mlynczak, M. G., Gordley, L. L., Tansock Jr, J. J., and Esplin, R. W.: Overview of  
786 the SABER experiment and preliminary calibration results, *Opt. Spectrosc. Tech. Instrum. Atmos. Sp.*  
787 *Res. III*, 3756, 277–288, 1999.
- 788 Russell III, J. M., Rong, P., Hervig, M. E., Siskind, D. E., Stevens, M. H., Bailey, S. M., and Gumbel,  
789 J.: Analysis of northern midlatitude noctilucent cloud occurrences using satellite data and modeling, *J.*



- 790 Geophys. Res. Atmos., 119, 3238–3250, 2014.
- 791 Schubert, G., Walterscheid, R. L., Hecht, J. H., and Sivjee, G. G.: Temperature gradients at  
792 mesopause heights inferred from OH nightglow data, *J. Geophys. Res. Sp. Phys.*, 95, 19061–19067,  
793 1990.
- 794 Seele, C. and Hartogh, P.: Water vapor of the polar middle atmosphere: Annual variation and summer  
795 mesosphere conditions as observed by ground-based microwave spectroscopy, *Geophys. Res. Lett.*,  
796 26, 1517–1520, 1999.
- 797 Seidel, D. J., Ross, R. J., Angell, J. K., and Reid, G. C.: Climatological characteristics of the tropical  
798 tropopause as revealed by radiosondes, *J. Geophys. Res. Atmos.*, 106, 7857–7878, 2001.
- 799 Semenov, A. I.: Long term temperature trends for different seasons by hydroxyl emission, *Phys.*  
800 *Chem. Earth, Part B Hydrol. Ocean. Atmos.*, 25, 525–529, 2000.
- 801 Semenov, A. I., Shefov, N. N., Lysenko, E. V., Givishvili, G. V., and Tikhonov, A. V.: The season  
802 peculiarities of behaviour of the long-term temperature trends in the middle atmosphere on the mid-  
803 latitudes, *Phys. Chem. Earth, Parts A/B/C*, 27, 529–534, 2002.
- 804 She, C.-Y., Krueger, D. A., Akmaev, R., Schmidt, H., Talaat, E., and Yee, S.: Long-term variability in  
805 mesopause region temperatures over Fort Collins, Colorado (41 N, 105 W) based on lidar  
806 observations from 1990 through 2007, *J. Atmos. Solar-Terrestrial Phys.*, 71, 1558–1564, 2009.
- 807 She, C.-Y., Krueger, D. A., and Yuan, T.: Long-term midlatitude mesopause region temperature trend  
808 deduced from quarter century (1990–2014) Na lidar observations, in: *Annales Geophysicae*, 363–369,  
809 2015.
- 810 She, C. Y. and Krueger, D. A.: Impact of natural variability in the 11-year mesopause region  
811 temperature observation over Fort Collins, CO (41 N, 105 W), *Adv. Sp. Res.*, 34, 330–336, 2004.
- 812 She, C. Y. and Von Zahn, U.: Concept of a two-level mesopause: Support through new lidar  
813 observations, *J. Geophys. Res. Atmos.*, 103, 5855–5863, 1998.
- 814 She, C. Y., Chen, S., Hu, Z., Sherman, J., Vance, J. D., Vasoli, V., White, M. A., Yu, J., and Krueger,  
815 D. A.: Eight-year climatology of nocturnal temperature and sodium density in the mesopause region  
816 (80 to 105 km) over Fort Collins, CO (41° N, 105° W), *Geophys. Res. Lett.*, 27, 3289–3292, 2000.
- 817 Siskind, D. E., Stevens, M. H., Hervig, M. E., and Randall, C. E.: Recent observations of high mass  
818 density polar mesospheric clouds: A link to space traffic?, *Geophys. Res. Lett.*, 40, 2813–2817, 2013.
- 819 Smith, A. K.: Physics and chemistry of the mesopause region, *J. Atmos. solar-terrestrial Phys.*, 66,  
820 839–857, 2004.
- 821 Solomon, S., Rosenlof, K. H., Portmann, R. W., Daniel, J. S., Davis, S. M., Sanford, T. J., and  
822 Plattner, G.-K.: Contributions of stratospheric water vapor to decadal changes in the rate of global  
823 warming, *Science (80-. )*, 327, 1219–1223, 2010.
- 824 Sonnemann, G. R., Grygalashvyly, M., and Berger, U.: Autocatalytic water vapor production as a  
825 source of large mixing ratios within the middle to upper mesosphere, *J. Geophys. Res. Atmos.*, 110,  
826 2005.
- 827 States, R. J. and Gardner, C. S.: Thermal structure of the mesopause region (80–105 km) at 40° N  
828 latitude. Part I: Seasonal variations, *J. Atmos. Sci.*, 57, 66–77, 2000.
- 829 Summers, M. E., Siskind, D. E., Bacmeister, J. T., Conway, R. R., Zasadil, S. E., and Strobel, D. F.:  
830 Seasonal variation of middle atmospheric CH<sub>4</sub> and H<sub>2</sub>O with a new chemical-dynamical model, *J.*  
831 *Geophys. Res. Atmos.*, 102, 3503–3526, 1997.





- 832 Le Texier, H., Solomon, S., and Garcia, R. R.: The role of molecular hydrogen and methane oxidation  
833 in the water vapour budget of the stratosphere, *QJ Roy. Meteor. Soc.*, 114, 281–295, 1988.
- 834 Thomas, G. E.: Are noctilucent clouds harbingers of global change in the middle atmosphere?, *Adv.*  
835 *Sp. Res.*, 32, 1737–1746, 2003.
- 836 Venkat Ratnam, M., Patra, A. K., and Krishna Murthy, B. V: Tropical mesopause: Is it always close  
837 to 100 km?, *J. Geophys. Res. Atmos.*, 115, 2010.
- 838 Vincent, R. A.: Gravity-wave motions in the mesosphere and lower thermosphere observed at  
839 Mawson, Antarctica, *J. Atmos. Terr. Phys.*, 56, 593–602, 1994.
- 840 Wallace, J. M. and Hobbs, P. V: *Atmospheric science: an introductory survey*, Elsevier, 2006.
- 841 Wang, N., Qian, L., Yue, J., Wang, W., Mlynczak, M. G., and Russell III, J. M.: Climatology of  
842 mesosphere and lower thermosphere residual circulations and mesopause height derived from SABER  
843 observations, *J. Geophys. Res. Atmos.*, 127, e2021JD035666, 2022.
- 844 Waters, J. W., Gustincic, J. J., Kakar, R. K., Kerr, A. R., Roscoe, H. K., and Swanson, P. N.: The  
845 microwave limb sounder experiment: Observations of stratospheric and mesospheric H<sub>2</sub>O in  
846 interhemispheric survey of minor upper atmospheric constituents during October–November 1976,  
847 *NASA Tech. Memo. TMX*, 73630, 1977.
- 848 Wörl, R., Strelnikov, B., Viehl, T. P., Höffner, J., Pautet, P.-D., Taylor, M. J., Zhao, Y., and Lübken,  
849 F.-J.: Thermal structure of the mesopause region during the WADIS-2 rocket campaign, *Atmos.*  
850 *Chem. Phys.*, 19, 77–88, 2019.
- 851 Wrotny, J. E., Nedoluha, G. E., Boone, C., Stiller, G. P., and McCormack, J. P.: Total hydrogen  
852 budget of the equatorial upper stratosphere, *J. Geophys. Res. Atmos.*, 115, 2010.
- 853 Xu, J., Liu, H., Yuan, W., Smith, A. K., Roble, R. G., Mertens, C. J., Russell III, J. M., and Mlynczak,  
854 M. G.: Mesopause structure from thermosphere, ionosphere, mesosphere, energetics, and dynamics  
855 (TIMED)/sounding of the atmosphere using broadband emission radiometry (SABER) observations,  
856 *J. Geophys. Res. Atmos.*, 112, 2007.
- 857 Yuan, T., Solomon, S. C., She, C., Krueger, D. A., and Liu, H.: The long-term trends of nocturnal  
858 mesopause temperature and altitude revealed by Na lidar observations between 1990 and 2018 at  
859 midlatitude, *J. Geophys. Res. Atmos.*, 124, 5970–5980, 2019.
- 860 Yue, J., Russell III, J., Gan, Q., Wang, T., Rong, P., Garcia, R., and Mlynczak, M.: Increasing water  
861 vapor in the stratosphere and mesosphere after 2002, *Geophys. Res. Lett.*, 46, 13452–13460, 2019.
- 862 Von Zahn, U. and Berger, U.: Persistent ice cloud in the midsummer upper mesosphere at high  
863 latitudes: Three-dimensional modeling and cloud interactions with ambient water vapor, *J. Geophys.*  
864 *Res. Atmos.*, 108, 2003.
- 865 Von Zahn, U. and Meyer, W.: Mesopause temperatures in polar summer, *J. Geophys. Res. Atmos.*,  
866 94, 14647–14651, 1989.
- 867 Zhao, X. R., Sheng, Z., Shi, H. Q., Weng, L. B., and Liao, Q. X.: Long-term trends and solar  
868 responses of the mesopause temperatures observed by SABER during the 2002–2019 period, *J.*  
869 *Geophys. Res. Atmos.*, 125, e2020JD032418, 2020.
- 870 Zhu, X., Yee, J., Talaat, E. R., Mlynczak, M., Gordley, L., Mertens, C., and Russell III, J. M.: An  
871 algorithm for extracting zonal mean and migrating tidal fields in the middle atmosphere from satellite  
872 measurements: Applications to TIMED/SABER–measured temperature and tidal modeling, *J.*  
873 *Geophys. Res. Atmos.*, 110, 2005.